Using El Niño to quantify cloud radiative feedback

by

Allison Kolly

A thesis submitted in conformity with the requirements
for the degree of Masters of Science
Department of Atmospheric and Oceanic Sciences
McGill University
Montreal, Quebec

Abstract

Using El Niño to quantify cloud radiative feedback

Allison Kolly

Masters of Science

Department of Atmospheric and Oceanic Sciences

McGill University

2017

There exists a prominent discrepancy between climate models and observations on the sign and magnitude of cloud radiative feedback during ENSO. Previous work, by Dessler (2013), showed that global climate models show a very strong, positive cloud feedback in the central Pacific which is not present in observations. To better understand this discrepancy and the role of radiation in ENSO cycle, we use the radiation data from the CERES satellite dataset and atmospheric data from the ERA-interim reanalysis dataset to diagnose the radiative energy budget. We extend the previous works by not only analyzing the TOA but also the surface and atmospheric radiation budgets, using a newly developed set of radiation kernels. We find that cloud radiative feedback plays an interesting role during the ENSO cycle, helping the thermal anomalies to develop and sustain. It is important for the global models to properly simulate the radiative energetic effects in order to improve their simulations of ENSO. Therefore, we draw comparisons to various prominent models representative of the CMIP5 model ensemble. Through this comparison, we observe that the models, on average, exhibit a positive bias at TOA which is not completely due to an overestimation of the longwave feedback, as previously thought, but also due to an underestimation of shortwave feedback.

Abstract

Using El Niño to quantify cloud radiative feedback

Allison Kolly

Masters of Science

Department of Atmospheric and Oceanic Sciences

McGill University

2017

Il existe un écart important entre les modèles climatiques et les observations à propos du signe et de l'amplitude de la rétroaction radiative des nuages pendant le cycle ENSO. Les travaux de Dessler (2013) montrent que les modèles climatiques globaux présentent une rétroaction causée par les nuage très forte et de signe positif dans le Pacifique central, qui n'est toutefois pas présente dans les observations. Afin de mieux comprendre cet écart et le rôle de la radiation atmosphérique dans le cycle ENSO, nous utilisons les données radiatives du satellite CERES et les données atmosphériques de la réanalyse ERA-interim pour faire un diagnostic du bilan radiatif. En effectuant une analyse du bilan radiatif à la surface et dans l'atmosphère, notre étude porte au-delà des travaux précédents qui s'intéressent uniquement au sommet de l'atmosphère. Nous développons à cette fin un nouvel ensemble de *kernels* radiatifs. Nous trouvons que la rétroaction radiative des nuages joue un rôle clé durant le cycle ENSO en contribuant à la formation et au maintien des anomalies de température. Il est donc important pour les modèles de représenter correctement les effets radiatifs afin d'améliorer les simulations d'ENSO. Dans cette perspective, nous établissons des comparaisons entre différents modèles représentatifs de l'ensemble multi-modèles CMIP5. Nous trouvons que les modèles présentent en moyenne un biais positif au sommet de l'atmosphère. Ce biais n'est cependant pas entièrement causé par une surestimation de la rétroaction du rayonnement aux ondes longues, comme supposé auparavant.

Acknowledgements

I would like to express many thanks to Yi Huang for supervising me during my Master's studies. He has given me many ideas and constructive comments over the past year and has been very helpful and encouraging. I would also like to thank the Atmospheric and Oceanic Sciences Department faculty and staff for all they have done in the past two years. To my parents, brother, and grandparents: thank you for your support, understanding and encouragement, not only during my studies, but thoughout my life. Finally, Tiago, thank you for the love you have shown me, especially in the times when I thought nothing was going right.

Contents

List of Tables

List of Figures

Chapter 1

A Review

1.1 General Overview

1.1.1 El Niño

El Niño is a very prominent feature in our current climate. The El Niño Southern Oscillation (ENSO) is a natural cycle that the Earth's climate undergoes; it occurs on a two to seven year timescale. An El Niño event is characterized by a sea surface temperature (SST) anomaly in the central Pacific greater than 0.5 K. Although this is the defining characteristic of an El Niño event, the effects of El Niño can be seen across the globe. These far-reaching effects are referred to as teleconnections - a correlation between meteorological or environmental phenomena. For example, during a typical El Niño year Eastern Canada and the Northeastern United states would experience an abnormally warm winter while the Western states, like California, are very wet during this time [1].

1.1.2 Causes and signs of El Niño

The ENSO cycle, itself, is made up of the warm El Niño event and its accompanying cold La Niña event with each lasting several months to several years. The variation between each phase is characterised by a shift in the Walker circulation (WC). The WC is used to describe the flow of air in the tropics over the Pacific Ocean. In a regular year in the ENSO cycle the central Pacific experiences easterly winds and the surface waters in the western Pacific are warm with cooler surface waters in the east off the coast of Peru. A non-El Niño year is also characterised by the presence of deep convective clouds over Indonesia.

An El Niño event is the result of a weakening, or reversed WC. This causes westerly surface winds and a higher than average SST in the central and eastern Pacific. The shifting winds also cause a shift in the location of the deep convective clouds. There is still some uncertainty in the exact role that these clouds play during an El Niño event, but it is likely that they are important in building up the SST anomaly.

1.1.3 Clouds and Radiation

It is known that clouds interact with radiation. What is unknown, however, is the magnitude of the effect of these interactions. Clouds interact with both longwave and shortwave radiation and the effect of each interaction plays a role in either heating or cooling the Earth's surface. What is unknown is which type of radiation plays the dominant role. Low, thick clouds reflect incoming solar radiation, cooling the Earth's surface, while high, thin clouds trap some of the outgoing infared radiation, warming the surface [2]. Therefore, a quantity worth studying is cloud feedback. By definition, cloud feedback is the cloud-related radiation anomaly that happens in response to a change in surface temperature.

To gain a full understanding of the role that clouds play we must study the response not only at the top of the atmosphere (TOA), but also at the surface and within the atmosphere, itself.

1.1.4 El Niño representation in models

There are an ensemble of Global Climate Models (GCMs) which are reviewed and their simulations archived by the Coupled Model Intercomparison Project Phase 5 (CMIP5). These models attempt to simulate the climate's response to various perturbations. Older model versions, archived by CMIP Phase 3 (CMIP3), were not able to accurately represent ENSO [3] and displayed a large bias which is not seen in observations. This bias can be attributed to a variety of factors including the way that the various feedbacks are represented in models.

1.2 Research objectives

The overall objective of this research is to better understand the role of clouds in the ENSO cycle.

Specifically, we wish to

- Quantify the total radiative anomalies.
- Isolate the cloud radiative feedback anomaly.
- Examine the radiative budgets at the top of the atmosphere (TOA), surface, and in the atmosphere.
- Examine how accurately models, representative of the CMIP5 ensemble, are able to represent the ENSO cycle.

1.3 Organisation of thesis and contribution of authors

The following remarks serve as a guide in reading this manuscript-based thesis.

Chapter 2 provides a detailed literature review on current discrepancies, the cloud feedback problem, and various radiation budgets.

Chapter 3 is a manuscript which will be submitted to *Journal of Geophysical Research*. This paper talks about the role of radiation in ENSO and discusses the importance of clouds in this cycle. This manuscript is a result of a collaborative work with Prof. Huang. I, Allison Kolly, executed the kernel method, as well as performed all of the statistical analysis, and wrote the manuscript describing the results. Prof. Huang provided the initial idea, supervised the research, and edited the manuscript. Some of the model simulation results were provided by Dr. Yan Xia.

Chapter 4 summarises the conclusions of the research performed.

Chapter 2

Literature review

2.1 Definition of El Niño

El Niño is the warming phase of the El Niño Southern Oscillation (ENSO). Through the years the exact definition of El Niño has changed [4]. Recently, a widely accepted definition defines El Niño as a large scale change in the interaction between the ocean and atmosphere which results in a warming of the sea surface temperature (SST) in the central equitorial Pacific [5]. ENSO, and thus, El Niño, are manifested by a change in the Walker circulation [6]. Under normal, non-El Niño, conditions deep, convective clouds reside over Indonesia whereas, during an El Niño year, the circulation change causes them to live over the central Pacific [7].

2.2 Radiation diagnosis of ENSO

In order to understand El Niño/ENSO we must have a good understanding the role of the atmospheric processes driving it. It is crucial to understand the important roles that radiation, and, in particular, cloud radiative feedback, play in the ENSO cycle. Within the context of ENSO two main conclusions have been drawn: (1) models underestimate the strength of negative shortwave cloud radiative forcing [8] and (2) they overestimate the positive feedbacks from radiative gases and water vapour [9]. [10] uses El Niño to study surface temperature variances in the cases of interactive and non-interactive clouds. They observe that the interactive cloud experiment had a surface temperature variance three times larger than the non-interactive cloud case. Furthermore, cloud radiative heating anomalies associated with El Niño warm the entire tropical atmosphere [10].

2.3 The Feedback Problem

Currently, a major issue is that there is much difficulty in quantifying cloud feedback. This is due to the fact that there are numerous cloud properties, including cloud amount, height, and optical depth [11], that need to be known in order to provide an accurate quantification. Another issue pertinent to this problem is the inability to accurately quantify feedbacks, in general, in the climate system [12]. More specifically, the way in which feedbacks are calculated varies between models.

There are a variety of methods used to quantify feedbacks in Global Climate Models (GCMs). One method, introduced by Wetherald and Manabe in [13], uses offline radiative transfer calculations to compute changes in radiative fluxes between two climate states [14]. The other method, developed by Cess et al. [15], [16] use sea surface temperature (SST) perturbations to change TOA fluxes. Although widely used, both of these methods have their drawbacks. While the first method is computationally expensive and has lead to differences in feedback calculations between groups, the second method does not isolate feedback effects of variables other than clouds [17].

A third method to analyze feedback, which is used in the analysis presented below, is the kernel method. The kernel-calculated feedbacks can be paired with observational results to subsequently analyze cloud feedback. The kernel method was developed by Soden et al. [17] as a means to quantify climate feedbacks. A mathematical description of this method is presented in chapter 3.

In this method, each meteorological variable has its own radiative kernel which is, essentially, the response of the longwave and shortwave fluxes to an incremental increase (in temperature, water vapour, etc.) [17]. The kernel method is superior in its feedback calculations since the kernels do not have a significant variation between models and it is computationally efficient [17] [18]. This technique is a straightforward way to compare radiative responses of different models [18].

In fact, many authors have looked in to the uncertainty of the radiative kernel method ([17], [19]). For TOA kernels all comparisons found that feedbacks from different sets of radiative kernels differed by an uncertainty of 10% or less [20]. While few surface kernels exist, a comparison can still be made between the three known products. Comparisons made in previous studies and tests of radiation closure [21] suggest that the kernel method can properly decompose the global mean radiation budget to within about 10% uncertainty level.

2.4 TOA and Surface Radiation Budgets

The main focus in the literature is on the TOA radiation balance. This is motivated by experiments such as the Earth Radiation Budget Experiment (ERBE) [22] and the Clouds and the Earth's Radiant Energy System (CERES) [11]. Both of these experiments provide measurements of the effect of clouds on the TOA radiation budget. Due to the accuracy with which we are now able to calculate the TOA radiation balance, it is possible to determine the incoming solar radiation to an accuracy of 0.035% [23]. The emitted thermal and reflected solar radiative fluxes more difficult to accurately quantify due to limitations in satellite instruments [24]. However, the authors are able to more accurately calculate these fluxes with the global mean shortwave and longwave TOA fluxes being 99.5 W m^{-2} and 239.6 W m^{-2}, respectively [24].

A downside to these satellite measurements is that they offer much less information regarding the surface and atmospheric radiation budgets which have to be computed. The difficulties in calculating the aforementioned budgets arise from the limitations of the input cloud properties and other information required for radiative transfer calculations [11]. Despite the difficulties there have been attempts by [25], [26], [27] and [28] to create a surface radiation budget.

In the past there were a variety of different approaches to deriving a surface radiation budget. One such approach was to develop a correlation between TOA radiative fluxes and surface fluxes to then derive a surface flux directly from satellite measurements [26]. These correlations have been found to work moderately well for the shortwave case [29]. However, this has been subject to criticisms. Alternatively, the longwave case has a narrow range of uses and does not work as well as for its shortwave counterpart. Another attempt at deriving a surface radiation budget was made by Trenberth and Caron [27] who interpret the surface fluxes to be a residual of the TOA measurements and atmospheric energy budget. Zhang et al. [28] also try to calculate the surface budget by using the International Satellite Cloud Climatology Project-C1 (ISCCP) data set.

A more recent attempt at this problem comes from Wild et al. [30]. The authors use observations as a mean of assessing the radiation budgets simulated in models within the Coupled Model Intercomparison Project Phase 5 (CMIP5) and further use surface observations to infer an estimate for the global mean surface radiative components. Through their detailed analysis, they are able to apply better constraints on the non-raditive components of sensible and latent heat.

An analysis of TOA radiation is common across all the literature. As discussed above, a topic not common in the literature is an accurate analysis of a surface and atmospheric radiation budget. We believe that we can accurately analyse the surface and atmospheric budgets through the use of surface kernels. A further study of this, as well as a comparison of observations to the latest Global Climate Models (GCMs), is a critical next step in understanding cloud radiative feedback.

2.5 Discrepancies between observations and models

There exists a discrepancy in the role that clouds play in our atmosphere. Both [3] and [12] have noticed a prominent regional model bias of the cloud feedback in the equitorial central Pacific. Furthermore, upon comparison to observations, [3] notes that a strong, positive feedback which is present in the models, but not in the observations. Although unknown, the source of the discrepancy could be related to how various feedbacks, including cloud feedback, are represented in the models. This thought is supported by Dufresne and Bony [31] who compare various feedbacks between 12 different models. In their work they find that the cloud feedback contribution has the greatest variability across all the models.

2.6 Missing Links

As discussed above, there are several gaps to be filled in order to gain a full understanding of the problem in question. Such holes include: discrepencies in radiative feedbacks between different models, and an incomplete understanding of the surface radiation budget. The analyses herein wish to improve the lack of understanding of the latter two, as well as provide a unique way to consider the atmospheric radiation budget.

Chapter 3

Data and methods

3.1 Observational Data

This work uses the SYN1deg-Month Edition3A observational data from the Cloud and Earth's Radiant System (CERES) instruments [32] and the ERA Interim (ERAi) Reanalysis data [33]. From the CERES instruments we use the measured TOA fluxes, while from ERAi we use their surface, and atmospheric temperature, specific humidity, and albedo fields. In order to keep our data consistent, and to reduce systematic error, we also use the ERAi computed surface fluxes. This consistency issue will be further discussed below. We also use a newly developed set of radiative kernels [21] to compute the radiative anomalies incurred by the meteorological variables.

All of the data has a 2.5×2.5 degree spatial resolution while the ERAi data also has 19 vertical layers. This resolution was chosen to match that of the kernels.

We use monthly mean data from March 2000 to September 2015 and define an anomaly to be the deviation from the 15-year climatological mean. This idea applies for the anomaly of a single month, and also for the three-monthly mean anomaly. Where the latter, for example the July-August-September (JAS) 2015 anomaly, is defined to be JAS_{2015} minus the 15-year mean of all JAS.

Above, we briefly mention the use of different data sets at TOA and at the surface. This was necessary in order to ensure consistency between radiation and non-radiation data. While it is known that the global averages of the CERES measured flux anomalies are in agreeance with the ERAi computed flux anomalies at TOA [34], it is not known whether or not the CERES and ERAi computed surface flux anomalies agree. Figure 3.1 acts to verify the TOA results found in figure 2 of [34]. It also demonstrates a considerable difference between the two datasets at the surface in terms of the inter-annual anomaly. Therefore, in order to ensure the consistency of between radiation and meteorological variables in our analysis, we use the ERAi computed fluxes for our surface analysis as they are computed in by the same forecast model as the ERAi meteorological variables. However, in doing so we limit the accuracy of our surface radiation analysis to the extent that ERAi represents reality.

It is important to note that every flux is defined to be downward positive. Therefore we may write:

$$R^{\text{NET}} = R^{\downarrow} - R^{\uparrow}. \tag{3.1}$$

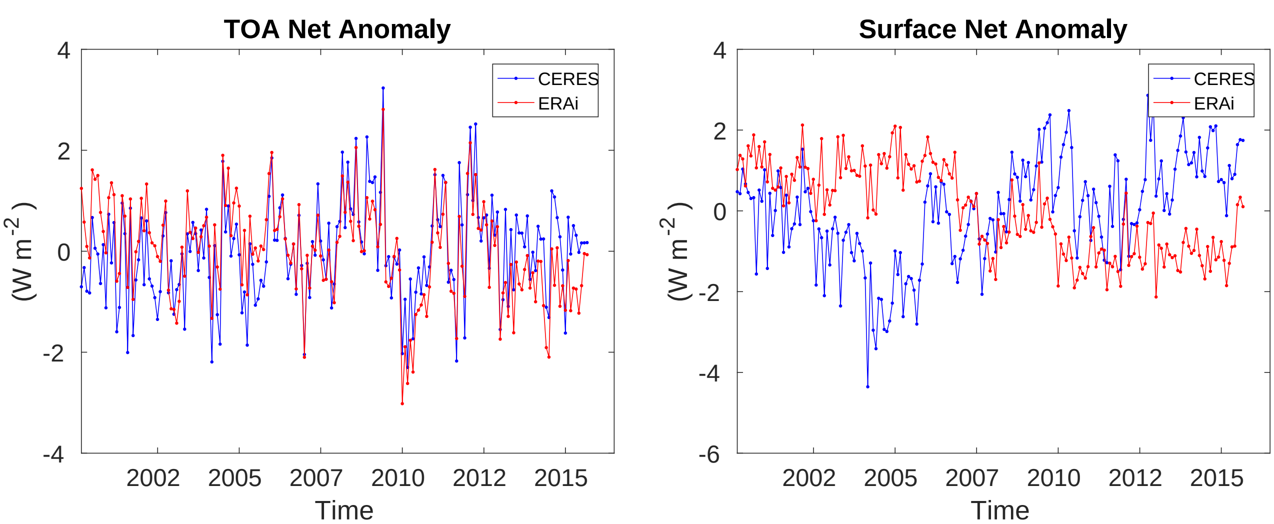

Figure 3.1: Monthly mean time series for tropical mean net radiation anomaly at TOA (left) and the surface (right) for all-sky conditions from March 2000 - September 2015 from CERES (blue) and ERAi (red) [Wm^{-2}].

3.2 GCM Data

In addition to studying the role of radiation during ENSO we also wish to compare observations to GCM simulations. To do so we look at a set of GCMs selected from the CMIP5 ensemble. First, we illustrate the GCM simulations with the Community Earth System Model (CESM) version 1.2 of the National Center of Atmospheric Research (NCAR) [35]. This is a fully coupled atmosphere-ocean GCM, and the data we use are the results of a 143-year control experiment in which the radiative gases (CO_2, CH_4, N_2, etc.) and aerosols are fixed at the year-2000 level [21]. From this point on, we will refer to this model as CESM-2000. We also look at data from a 318-year CESM experiment where the radiative gases are fixed at the year-1850 level (CESM-1850) from the CMIP5 archive. Other GCMs examined are control experiments from the Coupled Physical Model (CM3) from the Geophysical Fluid Dynamics Laboratory (GFDL) [36] (339 years), the NCAR Community Climate System Model version 4 (CCSM4) [37] (501 years), and the Hadley Centre Global Environment Model version 2 (HadGEM2) [38] from Met Office (240 years), for which the radiative gases are all fixed at pre-industrial levels.

3.3 The Kernel Method

We use a kernel method [17] to convert anomalies in temperature and humidity into radiative anomalies. This method separates feedback into two factors: (1) the radiative kernel, pre-calculated by the partial perturbation method i. e. by a small perturbation to a base climate variable and observing the TOA or surface response, and (2) the climate response simulated by each model. For the non-cloud climate variables, we compute the feedback as:

$$\Delta R_x = K_x \Delta X, \tag{3.2}$$

where K_x is the radiative kernel and ΔX is the climate response pattern, defined as the anomaly of each X variable.

In this analysis we use kernels at TOA, and we also use newly developed surface kernels; both computed by [21]. This allow us not only to study the surface radiation balance, but also to derive an overall atmospheric budget which is defined as

$$R^{\text{ATM}} = R^{\text{TOA}} - R^{\text{SFC}}, \tag{3.3}$$

where R are the fluxes. These three pieces, TOA, surface, and atmosphere, allow for a deeper look into the feedback given by clouds during an anomalous warming event.

To better understand the role of radiation, we can consider a typical tropical mean atmospheric and surface radiation anomaly during ENSO cycles which is on the order of 1 Wm^{-2}. A quick calculation shows that an anomaly of this magnitude roughly translates to about a 3K temperature change in a year for the whole atmospheric column, but merely 0.03K for a 250-metre ocean layer. It is clear that radiation, without a doubt, plays a significant role in the formation of the atmospheric energetics during ENSO. For the ocean, a larger anomaly is necessary to create significant impact, which is not the case for the tropical mean radiation, but is possible on regional scales (eg. the Niño 3.4 region).

However, as previously mentioned, ΔR_x in equation 3.2 only accounts for the non-cloud climate variables (temperature, humidity, etc.). To take the clouds into account we compute the cloud feedback as

$$\Delta R_{cld} = \Delta R - \sum_x \Delta R_x, \tag{3.4}$$

where ΔR is the CERES-observed or ERAi-computed total radiation anomlay.

3.4 Analysis Procedure

The work begins by first identifying anomalies in dynamic variables, such as temperature and humidity, and in the TOA radiation from ERAi and CERES, respectively. Once the anomaly patterns for the meteorological variables are identified, the kernel method can be applied in order to convert these into anomalies with radiation units at TOA.

Upon finding the radiative anomalies one can find the cloud effect at TOA by applying equation 3.4. This net result can be further decomposed into its longwave and shortwave components. From, here a series of statistical tests were performed on the data to quantitatively analyse the results; specifically, composite, regression and lagged regression analysis.

The procedure outlined above is then repeated in order to study radiative anomalies at the surface. However, a major difference exists between this analysis and that for the TOA. In the case of the surface analysis we opted to use surface fluxes computed by the ERAi product, instead of those from CERES with the reasoning having previously been discussed.

Once an analysis of the surface budget is complete, we can use it with the TOA budget to study the atmospheric budget of the radiation. The same statistical analyses are performed in order to obtain a conclusion about sign and magnitude of the cloud radiative effect.

3.5 Clear Sky Closure

Non-closure is define as the difference between calculated and measured radiation [39] and is important for testing the consistency between radiation and meteorological variables. Although beyond the scope of this thesis, studying closure in depth is key to making accurate retrievals and measurements of cloud properties [39]. We perform a brief study of the clear sky closure as a check to see if the kernel method can explain variability in fluxes.

At TOA, both the CERES clear-sky and kernel-calculated clear-sky data have similar patterns and have approximately the same magnitude. This is demonstrated in the upper rightmost image of figure 3.2. By subtracting the kernel-calculated fluxes from the CERES observed fluxes, the result is slightly negative. We can compare the clear sky closure using the CERES fluxes to that using the ERAi computed fluxes. The result being that the ERAi

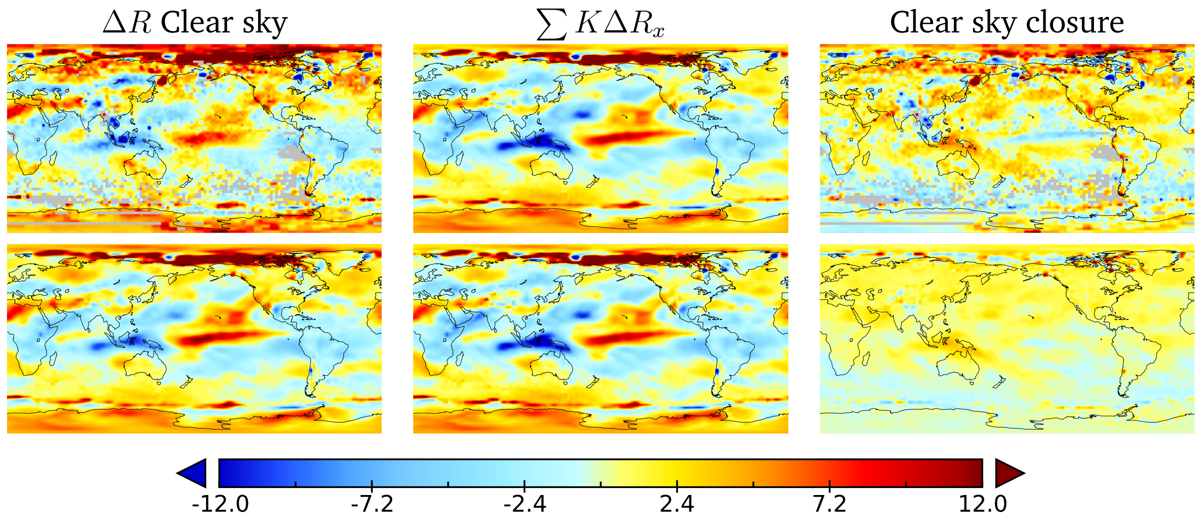

Figure 3.2: Clear-sky closure check of the JAS_{2015} three-monthly mean anomaly at TOA using the CERES flux anomaly (top) and ERAi flux anomaly (bottom) [$\text{Wm}^{-}2$].

fluxes demonstrate better closure over the central Pacific.

We see a similar result when we look at the computed surface fluxes. Figure 3.3 shows a much better closure at the surface using the ERAi computed fluxes. The closure result of the CERES fluxes offers a good explanation of the discrepency of the tropical mean net anomaly seen in figure 3.1. Globally, figure 3.3 shows that the overall difference between the ERAi fluxes and the kernel calculated fluxes is much more neutral across the entire map in comparison to the CERES fluxes. This result is mostly, if not entirely, due to the fact that the ERAi fluxes and meteorological variables are both computed in the same manner. Thus, we may use the results of figure 3.2 and 3.3 as evidence that the kernel method does a good job in explaining the flux variability.

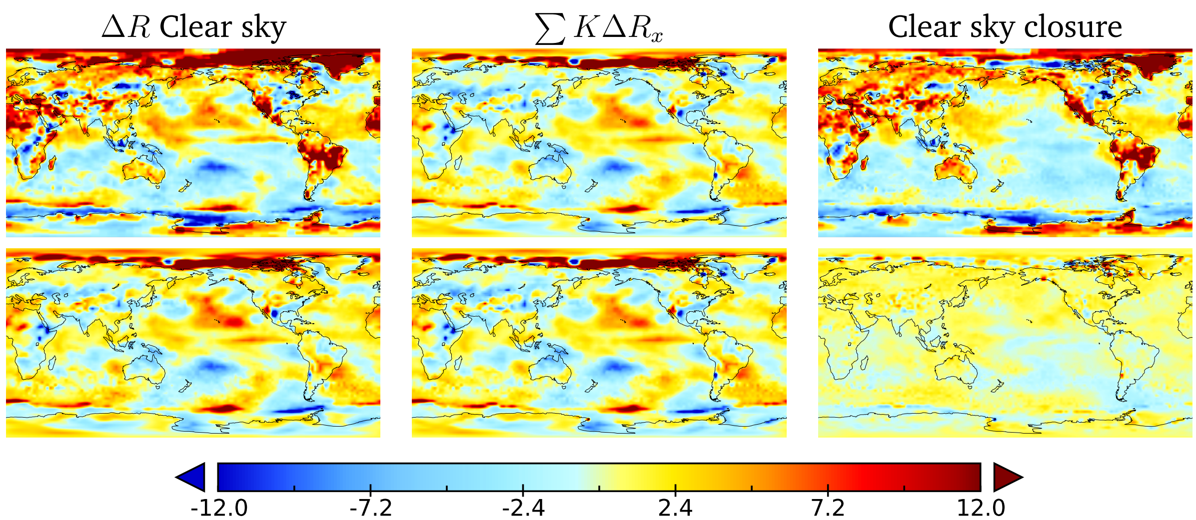

Figure 3.3: Clear-sky closure check of the JAS_{2015} three-monthly mean anomaly at the surface using the CERES flux anomaly (top) and ERAi flux anomaly (bottom) [Wm^{-2}].

Chapter 4

Results

Before we begin presenting results, we must first define some the order in which the results will be presented. The observational results will be presented first, followed by the model results and, unless otherwise stated, all model data presented in this paper are results from CESM-2000. This run is selected as the GHG concentrations are a more accurate representation of our current climate, and there is little difference between CESM-2000 and CESM-1850. Finally, a comparison will be made between the observations and the various models.

4.1 Observational Results

Figure 4.1 shows the observed total radiative anomaly, ΔR, regressed to the Niño 3.4 region mean SST. From this we get an idea of the overall radiative anomaly in the context of ENSO. An El Niño event is characterised by a shift in the Walker circulation and thus the presence of anomalous clouds in the central Pacific region. Therefore, we can hypothesise that the signals we are seeing over the central Pacific are caused by these anomalous clouds. The radiative anomalies that can be seen in figure 4.1 agree with this hypothesis.

The results of figure 4.1 can be further explained in the context of ENSO by looking at figure 4.2. Through the use of equation 3.4, we can isolate the radiative effect due to

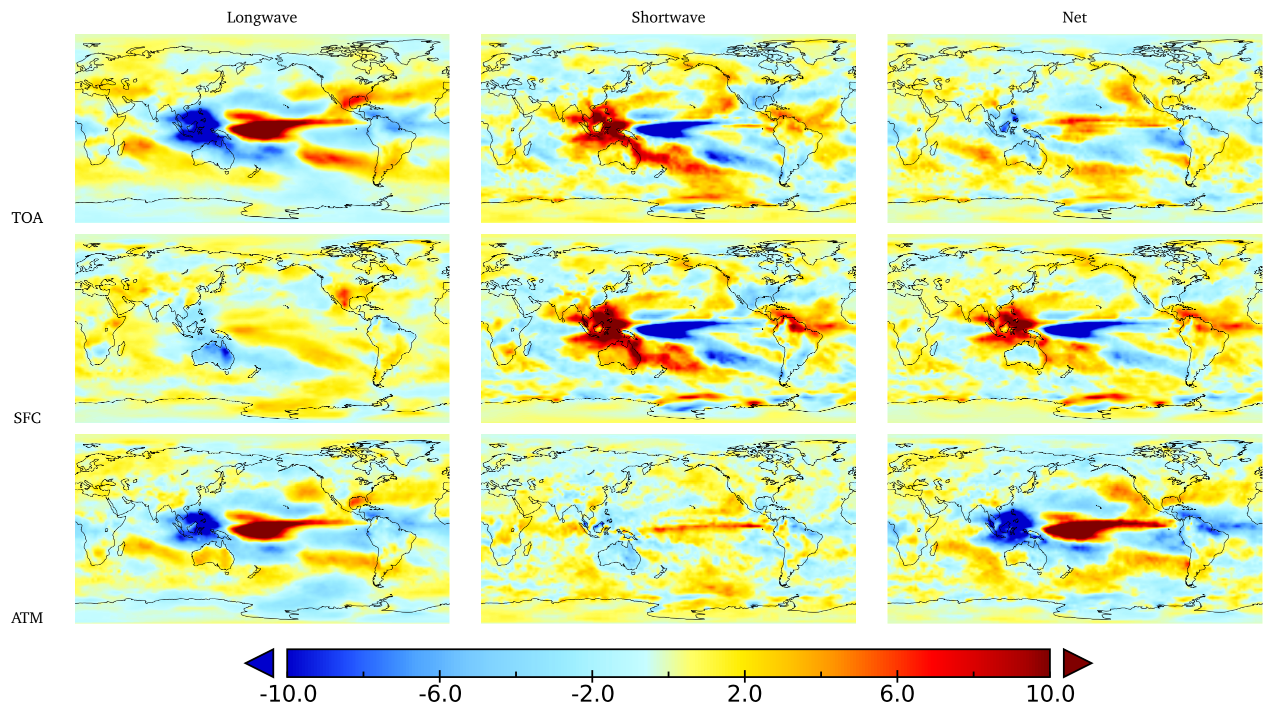

Figure 4.1: Observational total radiation anomaly regressed to the Niño 3.4 region mean SST [W m^{-2} K^{-1}]

clouds in order to quantify its magnitude.

At TOA see that the net cloud radiative feedback anomaly neutralised over the central Pacific. This is due to a balance between the longwave and shortwave cloud radiative anomalies. Meanwhile, at the surface, we see that the net anomaly is dominated by a strong shortwave cooling. Thus, the overall response that the atmosphere experiences is a positive, warming one.

The signals that we see when we isolate the radiative effect due to clouds is well explained by anomalous clouds present during an El Niño event. The positive longwave and negative shortwave signals at TOA are indicative of a trapping and reflection of thermal radiation, and a reflection of solar radiation respectively. At the surface, there is a strong decrease of shortwave radiation as less is reaching the surface due to the presence of clouds.

Figure 4.3 shows the result of the kernel-calculated radiative feedbacks due to the

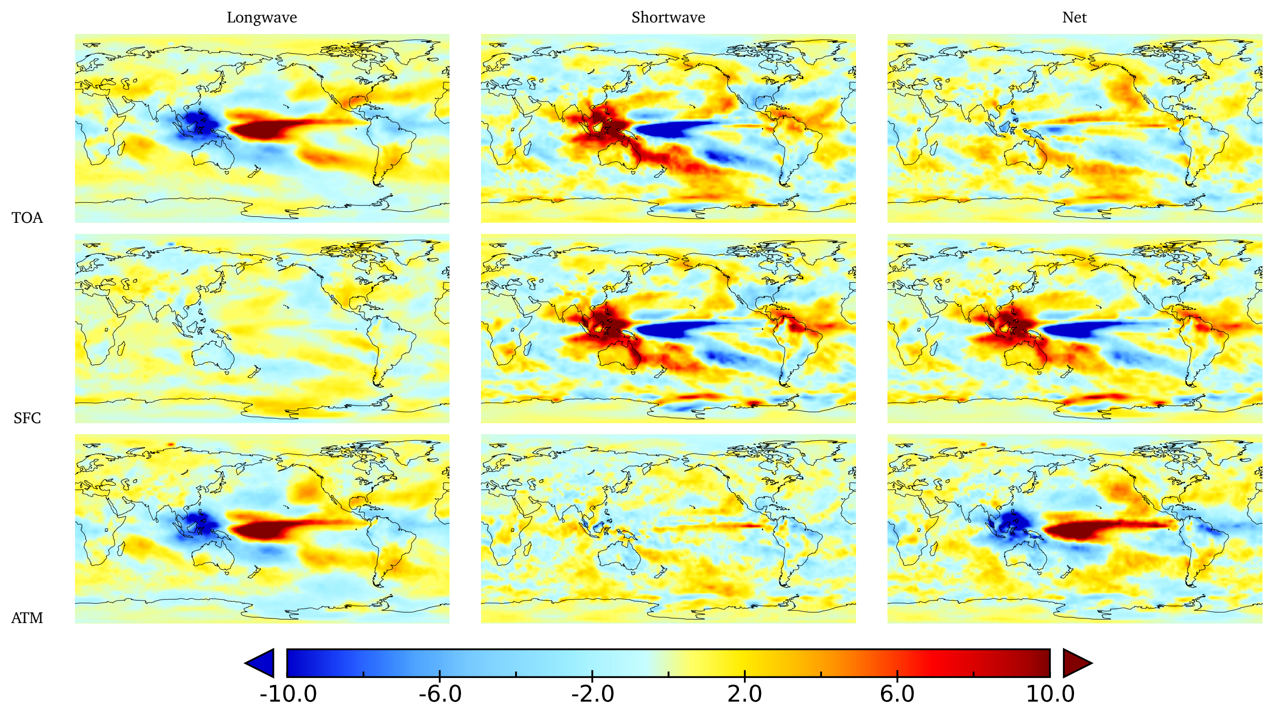

Figure 4.2: Observational cloud radiative feedback regressed to the Niño 3.4 region mean SST [W m^{-2} K^{-1}]

meteorological variables regressed to the Niño 3.4 region mean SST. We denote these feedbacks as λ_T and λ_Q which are the radiative anomalies associated with temperature and water vapour, respectively. At TOA, and within the atmosphere, λ_T, which is composed of both the atmospheric and surface temperature feedbacks, is largely influenced by the atmospheric temperature feedback. This is apparent through the dumbbell-pattern that we see to the North and South of the central Pacific. This dumbbell-shaped pattern is well known in the literature. Not only does it appear in the radiative anomaly due to the atmospheric temperature, but it also appears in the temperature field anomaly itself. This pattern is closely linked with a pattern of deep convection over the central Pacific and resembles the linear response to an equatorial heat source with an eastward shift [40].

Figure 4.3 also shows a strong atmospheric feedback signal in the central Pacific due to the interaction of both longwave and shortwave radiation with water vapour. This is not an unusual finding as we have already stated that, during El Niño, deep convective clouds

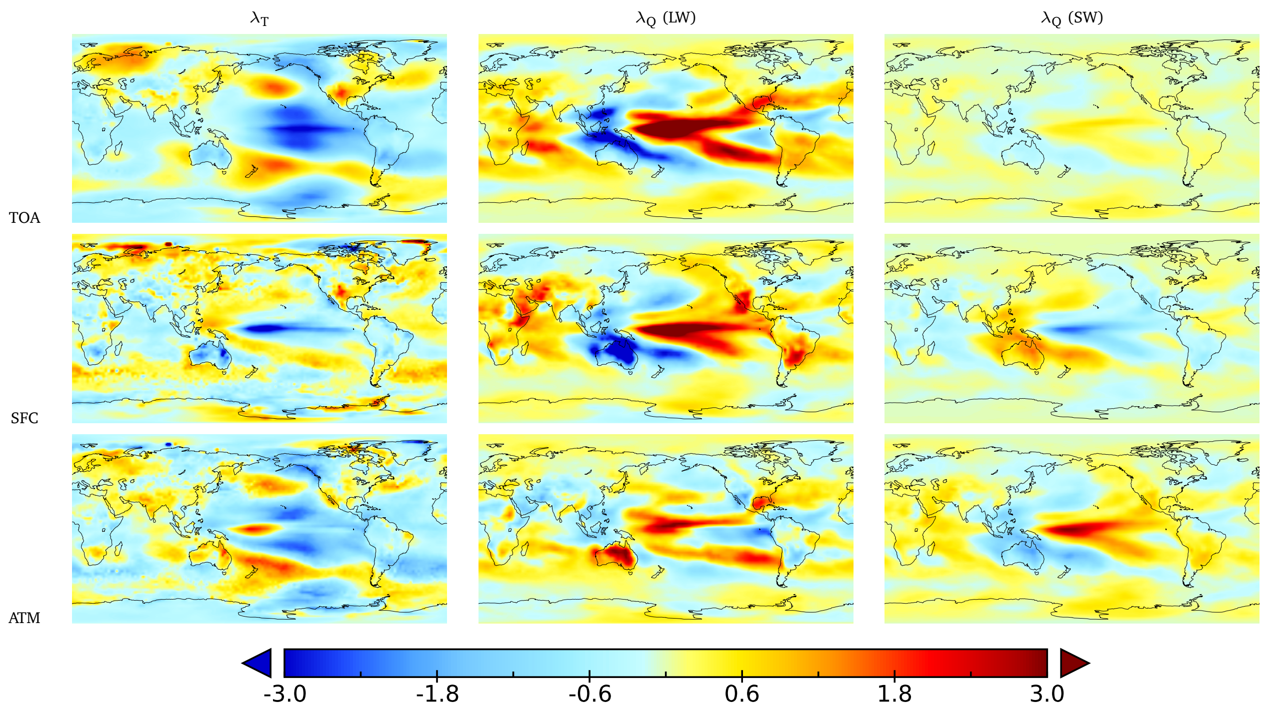

Figure 4.3: Kernel-calculated radiative feedbacks of ERAi meteorological variables regressed to the Niño 3.4 region mean SST [W m^{-2} K^{-1}]

reside over the central Pacific.

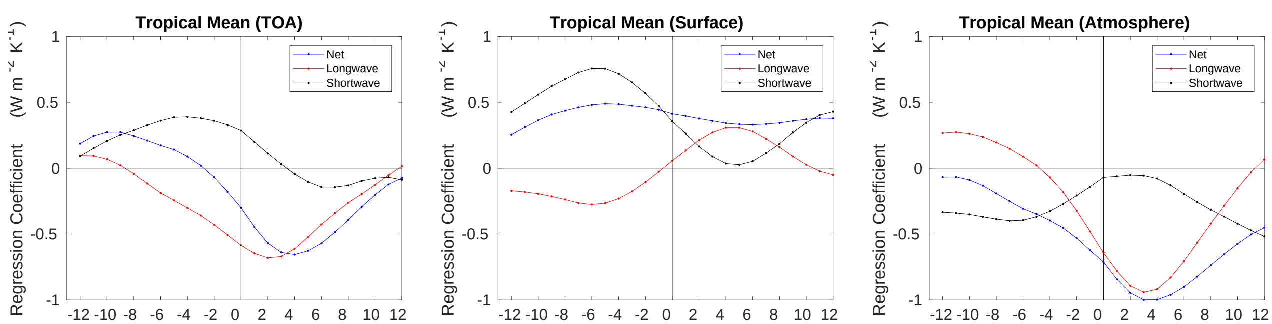

Figure 4.4: Lagged regression curves of the CERES (TOA) and ERAi (surface) tropical mean radiative anomaly regressed to the Niño 3.4 region mean SST [W m^{-2} K^{-1}]

To look further into the role played by radiation during different phases of ENSO we perform a lagged regression and look at the area-mean response. In doing so, we are able to look at the relationship between the radiative anomaly and the SST throughout the ENSO cycle. To calculate the lagged regression, we first create a lagged (from -12 to 12 month) Oceanic Niño Index (ONI) time series and then regress each three monthly-mean anomaly to the lagged ONI vector. The ONI is a three-month running mean of SST anomalies in the Niño 3.4 region [41].

Thus, the lagged linear regression takes the form

$$y = ax + b, \tag{4.1}$$

where y is a matrix of the radiative anomalies, with units of Wm^{-2}, x is a vector of the running mean ONI values, with units of K, and a represents the regression coefficient, with units of $\text{Wm}^{-2}\text{K}^{-1}$. Essentially, we are solving for the lagged coefficient values, a, which gives the relationship between our various radiative anomalies, and the Niño 3.4 Region SST anomalies. Here, we examine the tropical mean, and in sections 4.3 and 4.4 we look at the Niño 3.4 region mean.

Figure 4.4 looks at the tropical mean radiative response per Kelvin warming for the radiative anomaly through a 25 month cycle. Note that we define the tropics as the latitude band between 30° North and 30° South. What we notice at TOA is that the net regression coefficient (λ_{net}) transits from positive to negative. At the surface, the net radiative anomaly is positive which implies that in the tropical mean, we will see a negative λ_{net} in the atmosphere. Therefore, if we think back to our back-of-the-envelope calculation, in which an atmospheric radiation anomaly of magnitude 1 Wm^{-2} corresponds to a 3K warming, we can conclude that during the ENSO cycle the radiation anomaly causes a cooling in the tropical region of the atmosphere.

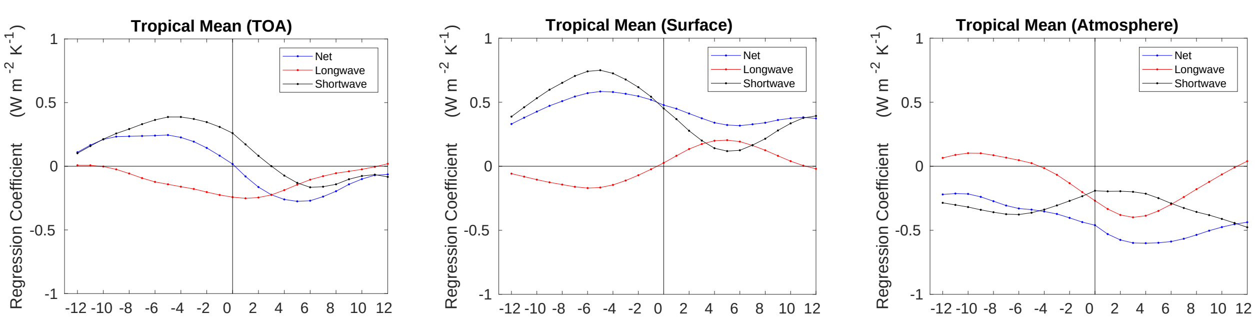

Figure 4.5: Lagged regression curves of the tropical mean observational cloud radiative feedback using CERES(TOA) and ERAi (surface) fluxes regressed to the Niño 3.4 region mean SST [W m^{-2} K^{-1}]

Figure 4.5 displays a similar behaviour for λ_{net} at TOA. This behaviour indicates that, at TOA, the radiation anomaly due to clouds acts to build, and then maintain, a positive temperature anomaly.

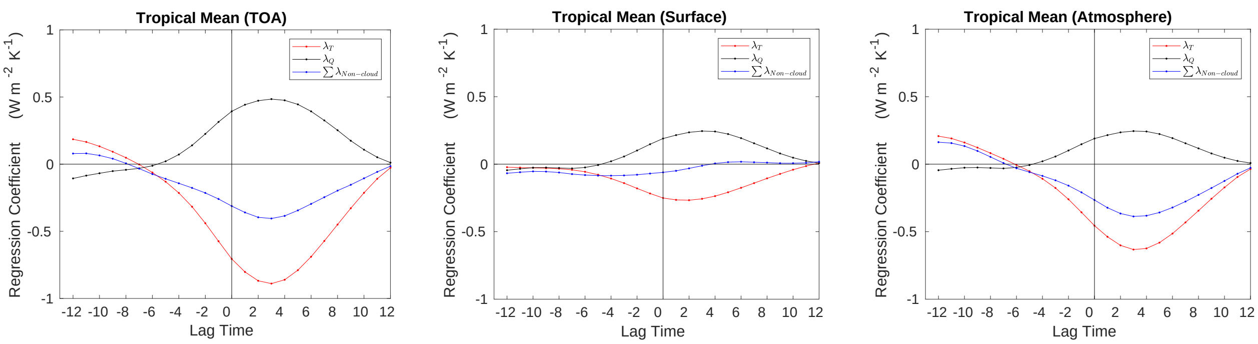

Figure 4.6: Lagged regression curves of the tropical mean kernel-calculated, ERAi meteorological variable fluxes regressed to the Niño 3.4 region mean SST [W m^{-2} K^{-1}]

Finally, we consider the regression of the radiative effects of the meteorological variables, T and Q to the ONI, shown in figure 4.6. Consistent with the conclusions we drew from figure 4.5, we see the temperature feedback (λ_T), which includes both the atmospheric and surface temperature feedbacks, peaks just after an El Niño event. We also see that at TOA the longwave and shortwave temperature and water vapour feedbacks are important in the tropical mean. The temperature feedback also has a large perturbation in the atmospheric tropical mean. Recalling the back of the envelope calculation, a perturbation of this magnitude will have a significant effect on the atmospheric heating rate.

Overall, what we can conclude from figures 4.4 - 4.6 is that the radiative feedback, itself, does have a large effect in the tropical mean in the atmosphere during the different phases of ENSO. This radiative anomaly is due to the cloud radiative effect, and to the radiative effect of the meteorological variables, as well.

4.2 GCM Results

We next look to various models to see how well they represent the ENSO cycle. In doing so, we wish to investigate the discrepency in the cloud radiation feedback as observed by [3] and see if the positive bias observed persists in the CMIP5 models. Shown below are the results of the CESM-2000 simulation. Henceforth, "the model" refers to the CESM-2000 simulation.

Before even considering the model's cloud radiative feedback, figure 4.7 clearly demonstrates an overestimation of the radiative fluxes at TOA and the surface over the central Pacific. Despite this, the patterns of different components seen are a good replication of those in figure 4.1. However, one will immediately notice an overestimation of λ_{net} at TOA, especially in the Eastern Pacific, due to a too-large λ_{LW}.

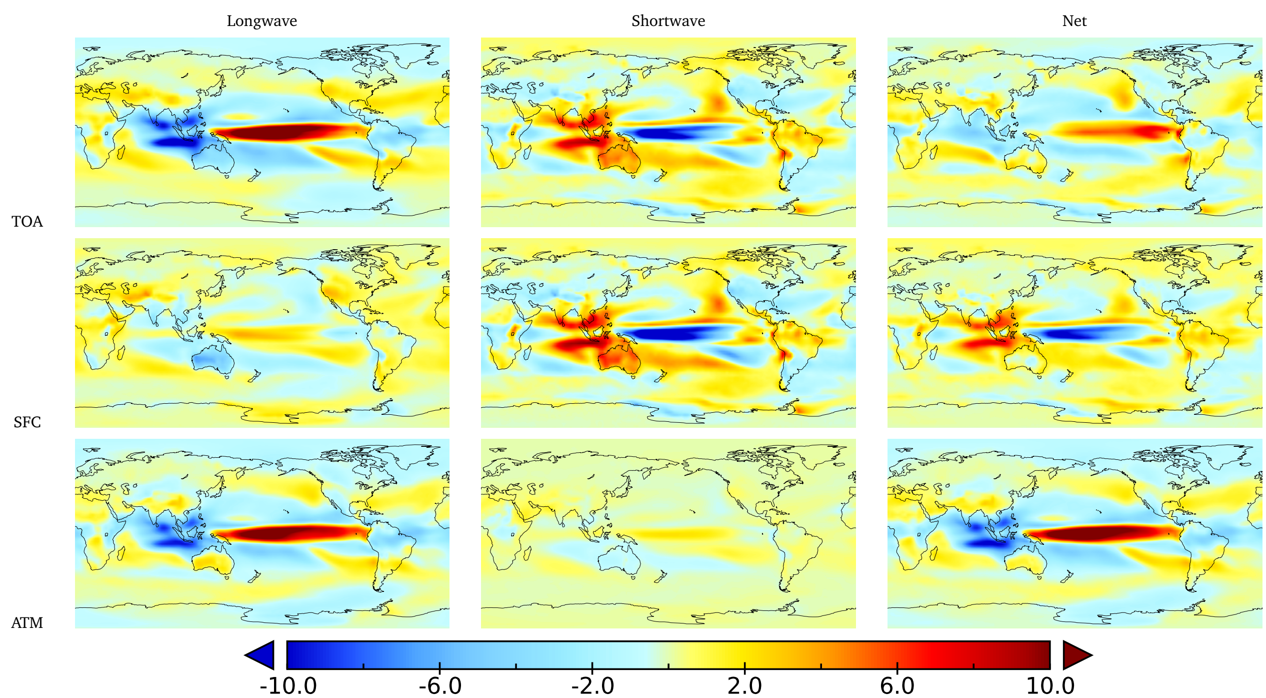

Figure 4.7: CESM-2000 total radiation anomaly regressed to the model Niño 3.4 region mean SST [W m^{-2} K^{-1}]

Figure 4.8 displays the results of regressing the cloud radiative feedback to the model's Niño 3.4 region mean SST. Comparing the results to those of figure 4.2 we notice a prominent positive bias of $\lambda_{\text{net}}^{\text{cloud}}$ in the central and Eastern Pacific at TOA where, in the observations, the cloud feedback signal is fairly neutralised. The cause of this TOA bias is a too-strong longwave signal in the atmosphere.

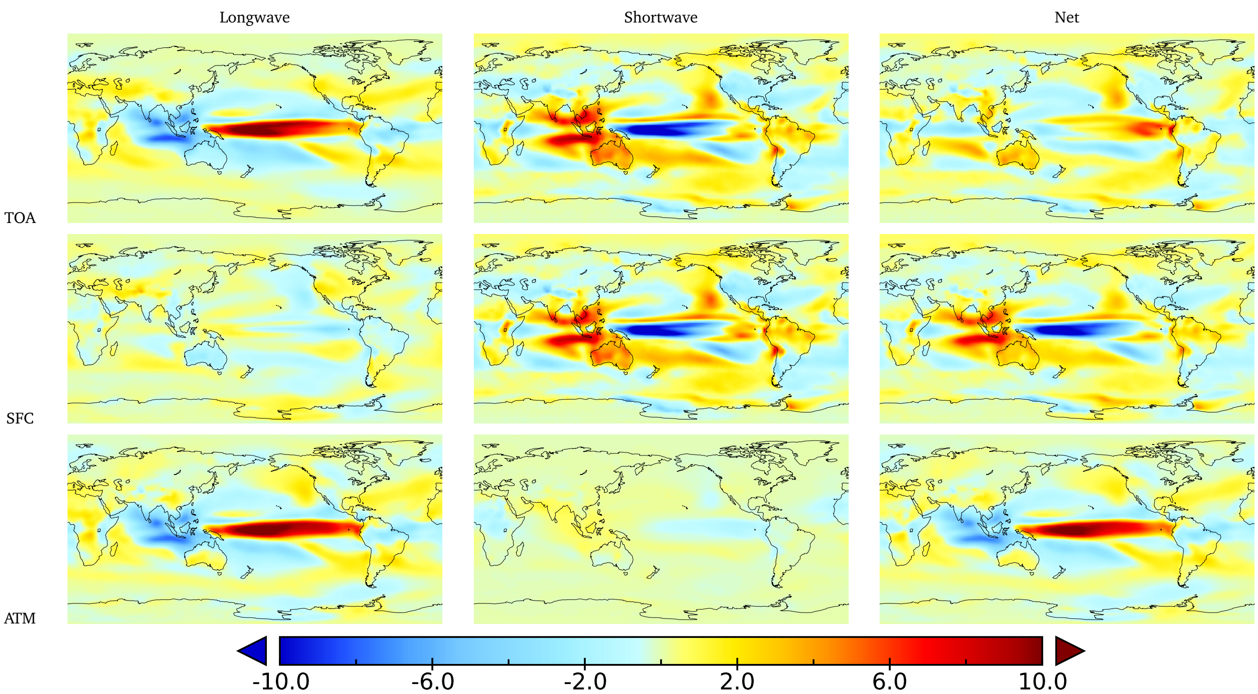

Figure 4.8: CESM-2000 cloud radiative feedback regressed to the model's Niño 3.4 region mean SST [W m^{-2} K^{-1}]

By using figures 4.7 and 4.8 we can infer that the overestimation of the TOA longwave component is largly due to the magnitude of the atmospheric longwave radiation anomaly. This thought can be further confirmed by investigating the radiative effects of the meteorological variables, T and Q.

Figure 4.9 shows the meteorological variables of the model regressed to the model's Niño 3.4 region mean SST. For λ_T at TOA, the model fails to accurately represent the "dumbbell" pattern seen in observations. What we do see, however, is a fairly good representation of all other aspects of λ_T and λ_Q at all levels.

We can next look at how the model's various fluxes and feedbacks behave during an ENSO cycle. Figure 4.10 shows a lagged regression of the model fluxes. In all three panels we observe a similar pattern to that of figure 4.4. One major discrepancy is the

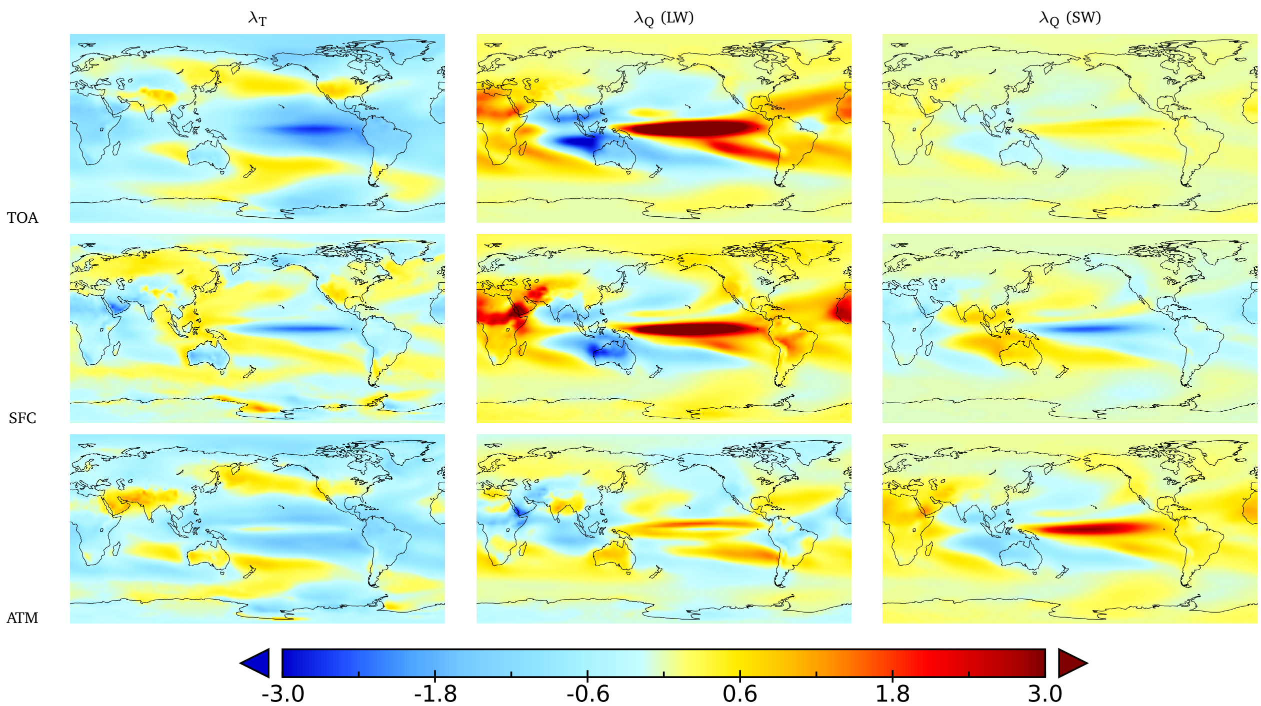

Figure 4.9: Atmospheric variables from CESM-2000 regressed to the Niño 3.4 region mean SST [W m^{-2} K^{-1}]

model estimation of the surface shortwave component which results in a positive, warming shortwave signal the atmospheric tropical mean throughout most of the ENSO cycle.

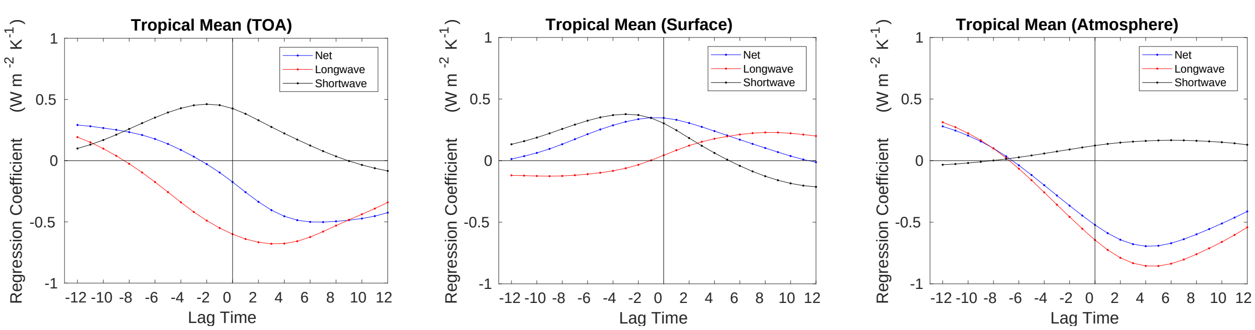

Figure 4.10: Lagged regression curves of the CESM-2000 tropical mean net fluxes regressed to the Niño 3.4 region mean SST [W m^{-2} K^{-1}]

Figure 4.11 is the result of a lagged regression of the CESM1.2 cloud feedback to the model's Niño 3.4 region mean SST. Comparing to figure 4.5 we see that the GCM is a good representation of the TOA cloud feedback. However, in the atmosphere we observe very small perturbations in cloud feedback through the ENSO cycle. Therefore, in the model's atmosphere, the clouds play a minimal role.

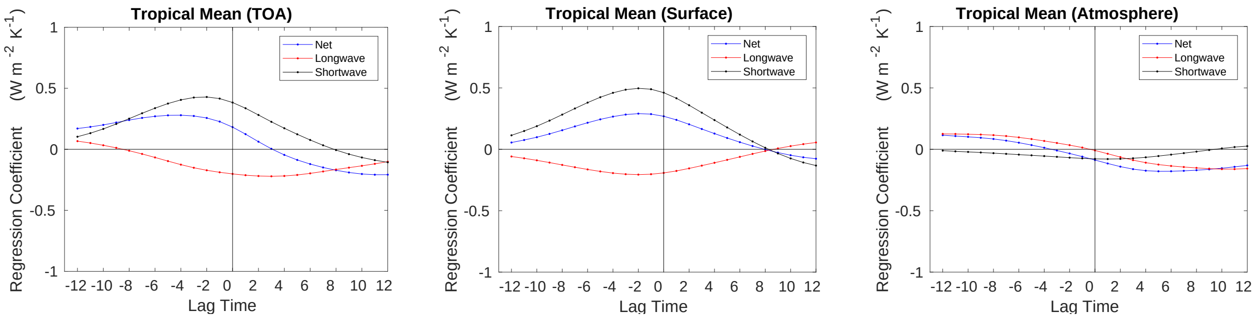

Figure 4.11: Lagged regression curves of the CESM-2000 tropical mean cloud radiative feedback regressed to the Niño 3.4 region mean SST [W m^{-2} K^{-1}]

Finally, we look at the model's λ_T and λ_Q, shown in figure 4.12 and draw comparisons to the observations, figure 4.6. The CESM-2000 model does a good job at replicating the patterns seen in figure 4.6 and does fairly well at representing the magnitudes.

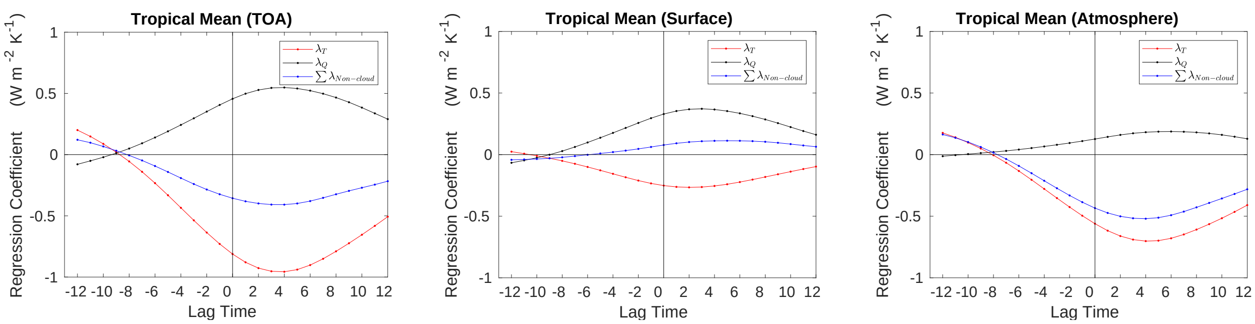

Figure 4.12: Lagged regression curves of the tropical mean, kernel-calculated, CESM-2000 meteorological variables fluxes regressed to the Niño 3.4 region mean SST [W m^{-2} K^{-1}]

4.3 Inter-model comparison

What we have seen so far is the result of one model's data. We can perform an inter-model comparison to statistically assess how various models compare to one another. Figure 4.13 shows the inter-model mean of the CESM-2000, CESM-1850, CCSM, HadGEM, and GFDL-CM3 control. We see that the net positive bias in the central/eastern Pacific at TOA is not unique to the CESM-2000 results that were presented above.

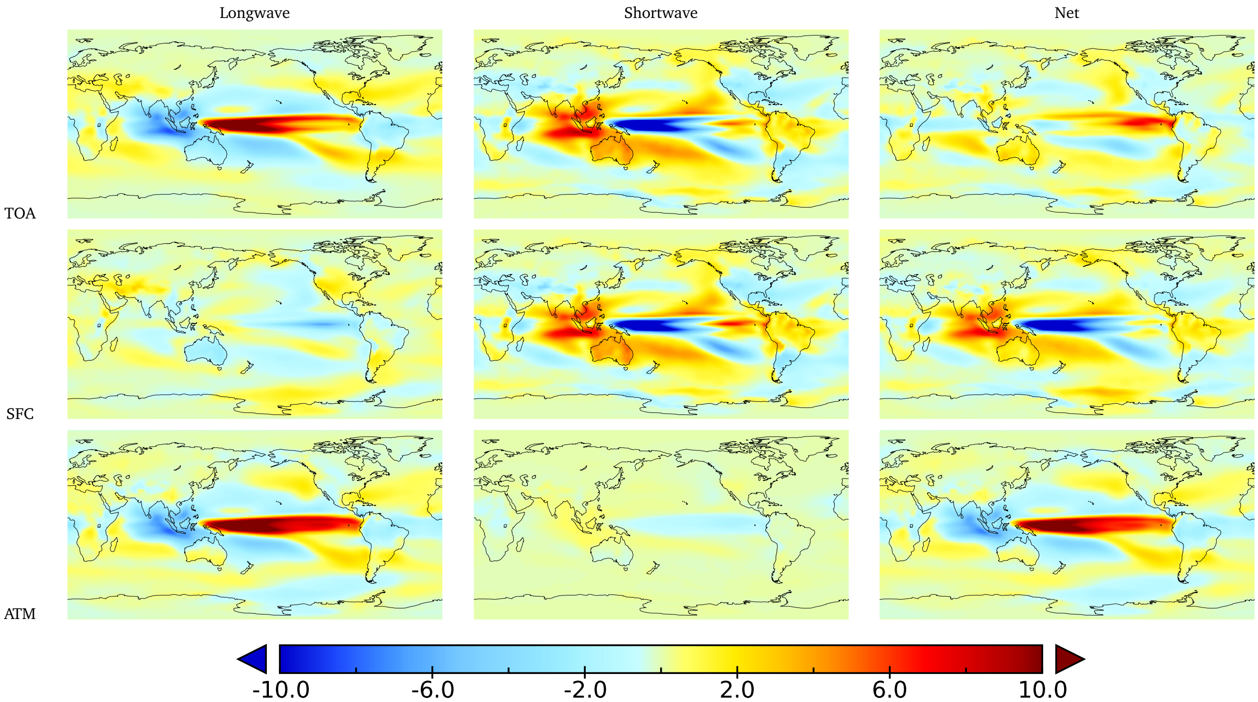

Figure 4.13: Inter-model mean cloud radiative feedback regressed to each model's Niño 3.4 region mean SST [W m^{-2} K^{-1}]

The inter-model mean, figure 4.13, shows us that the mean of multiple models displays a positive bias in the central Pacific. We can further investigate this bias by looking at the inter-model mean, μ, and standard deviation, σ, of both the tropical and the Niño region means and comparing to their corresponding observational means. μ and σ are calculated by taking the regional mean of each model.

Tables 4.1 and 4.2 show the inter-model mean of the tropical and Niño region means, respectively, compared to the observations. The tropical mean shows an underestimation of the longwave, and overestimation of the shortwave components. However, based on σ_{GCM}, we see that the models all have a similar representation of ΔR in the tropical mean.

Meanwhile, table 4.2 displays the Niño region mean and standard deviation of the models where, again, we see an underestimation of the longwave, and overestimation of the shortwave components. This time, σ_{GCM} is consistently quite large which gives evidence for the presence of regional discrepancies.

	Longwave			Shortwave			Net		
	Obs	μ_{GCM}	σ_{GCM}	Obs	μ_{GCM}	σ_{GCM}	Obs	μ_{GCM}	σ_{GCM}
TOA	-0.59	-0.47	0.09	0.29	0.48	0.19	-0.30	0.01	0.18
SFC	0.06	-0.01	0.07	0.36	0.39	0.21	0.41	0.38	0.15
ATM	-0.64	-0.46	0.11	-0.07	0.09	0.05	-0.71	-0.37	0.09

Table 4.1: Inter-model mean and standard deviation of the tropical mean regressed radiative feedback as compared to the observations [$\text{Wm}^{-2}\text{K}^{-1}$].

	Longwave			Shortwave			Net		
	Obs	μ_{GCM}	σ_{GCM}	Obs	μ_{GCM}	σ_{GCM}	Obs	μ_{GCM}	σ_{GCM}
TOA	6.36	8.69	3.46	-4.74	-3.49	4.79	1.62	5.20	2.43
SFC	0.89	0.81	1.84	-7.58	-4.44	5.15	-6.69	-3.64	3.55
ATM	5.47	7.88	2.80	2.84	0.95	0.58	8.31	8.83	2.64

Table 4.2: Like table 4.1, but for the Niño region mean regressed radiative feedback[$\text{Wm}^{-2}\text{K}^{-1}$].

Tables 4.3 and 4.4 showthe inter-model μ and σ cloud radiative feedback. For the tropical mean, table 4.3, we see that the models' have a very good estimate of the λ_{LW}, but overestimate λ_{SW} at TOA and the surface. The inter-model Net μ_{GCM} does not well represent observations.

At TOA in table 4.4 we notice a very strong positive longwave signal and a weaker, negative shortwave signal, relative to the observational counterparts, which cause a net positive bias. At the surface we see a similar result: a large overestimation of the longwave component, and an underestimation of the shortwave component. Interestingly, both at TOA and at the surface, σ_{GCM} is larger than the inter-model mean - indicative of a large spread of values. This being said, σ_{SW} in the atmosphere is relatively small.

	Longwave			Shortwave			Net		
	Obs	μ_{GCM}	σ_{GCM}	Obs	μ_{GCM}	σ_{GCM}	Obs	μ_{GCM}	σ_{GCM}
TOA	-0.24	-0.17	0.09	0.26	0.44	0.19	0.02	0.27	0.16
SFC	0.03	-0.26	0.36	0.45	0.52	0.21	0.48	0.26	0.27
ATM	-0.27	0.09	0.28	-0.19	-0.08	0.04	-0.46	0.01	0.24

Table 4.3: Like table 4.1, but for the tropical mean regressed cloud radiative feedback[$\text{Wm}^{-2}\text{K}^{-1}$].

	Longwave			Shortwave			Net		
	Obs	μ_{GCM}	σ_{GCM}	Obs	μ_{GCM}	σ_{GCM}	Obs	μ_{GCM}	σ_{GCM}
TOA	5.69	6.31	3.02	-5.09	-3.91	4.82	0.61	2.40	2.03
SFC	-0.16	-2.29	3.84	-6.33	-2.82	5.14	-6.49	-5.11	3.18
ATM	5.85	8.60	3.25	1.24	-1.09	0.62	7.10	7.51	2.74

Table 4.4: Like table 4.1, but for the Niño region mean regressed cloud radiative feedback[$\mathrm{Wm}^{-2}\mathrm{K}^{-1}$].

4.4 Comparison of observations and models

So far we have seen the observational and model results on their own, as well as looked at a model inter-comparison in which we identify the inter-model mean and standard deviation of the tropical and Niño region means of the five experiments that we examined. We have also identified that the Niño 3.4 region in the most of the models exhibits an strong positive bias relative to observations. Therefore, it is useful to expand on the results of section 4.3 by comparing both the observation and various models' tropical and Niño 3.4 region mean radiative, and cloud radiative feedbacks through the ENSO cycle.

We will first look at the ΔR comparisons of the tropical and Niño region means shown in figures 4.14, and 4.15, respectively. At TOA for the tropical mean we see that the the models do a good job of replicating the pattern seen in the observations. Furthermore, at TOA and in the atmosphere, we see that, while the overall pattern is well replicated, the magnitude of the net flux is not. What we see in the Niño region consistently is a good representation of the feedback patterns with a poor representation of magnitudes.

The tropical mean comparison of the cloud radiative feedback is shown in figure 4.16. Here we see that the models' net cloud feedback, in general, is too positive at TOA and in the atmosphere. From this, we can see that the models do not correctly replicate the regional compensations as the negative and positive feedback regions are due to systematic movement of convections. This is also due to a too positive longwave atmospheric feedback.

Figure 4.17 shows the comparison of the Niño region mean cloud radiative feedback

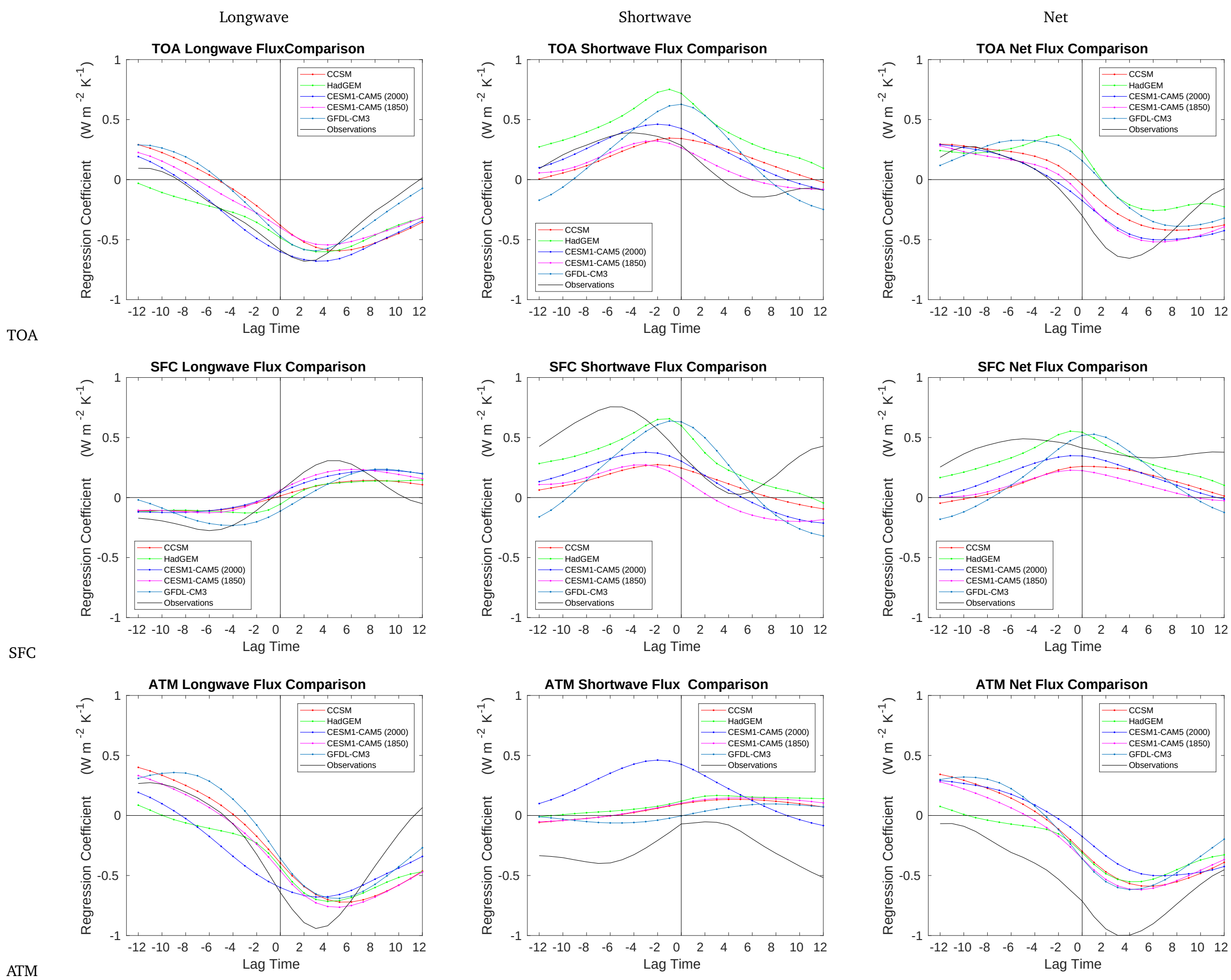

Figure 4.14: Lagged regression comparison between observations (black) and models of the tropical mean radiative feedback regressed to to the Niño 3.4 region mean SST [W m^{-2} K^{-1}].

through the ENSO cycle. The positive bias that we see at TOA in figure 4.8 is very clearly illustrated in the TOA net comparison, especially in the HadGEM and GFDL simulations.

However, despite the overall net cloud radiative feedback of the models having a positive bias, we can further see that the CCSM control simulation has a bias which is less positive than the observations. This less positive bias persists throughout the various phases of ENSO and results in the CCSM simulation having an overall neutral pattern. What is interesting is that the positive bias at TOA that is seen in most models cannot be entirely attributed to a longwave bias. In fact, for the HadGEM and GFDL simulations we notice

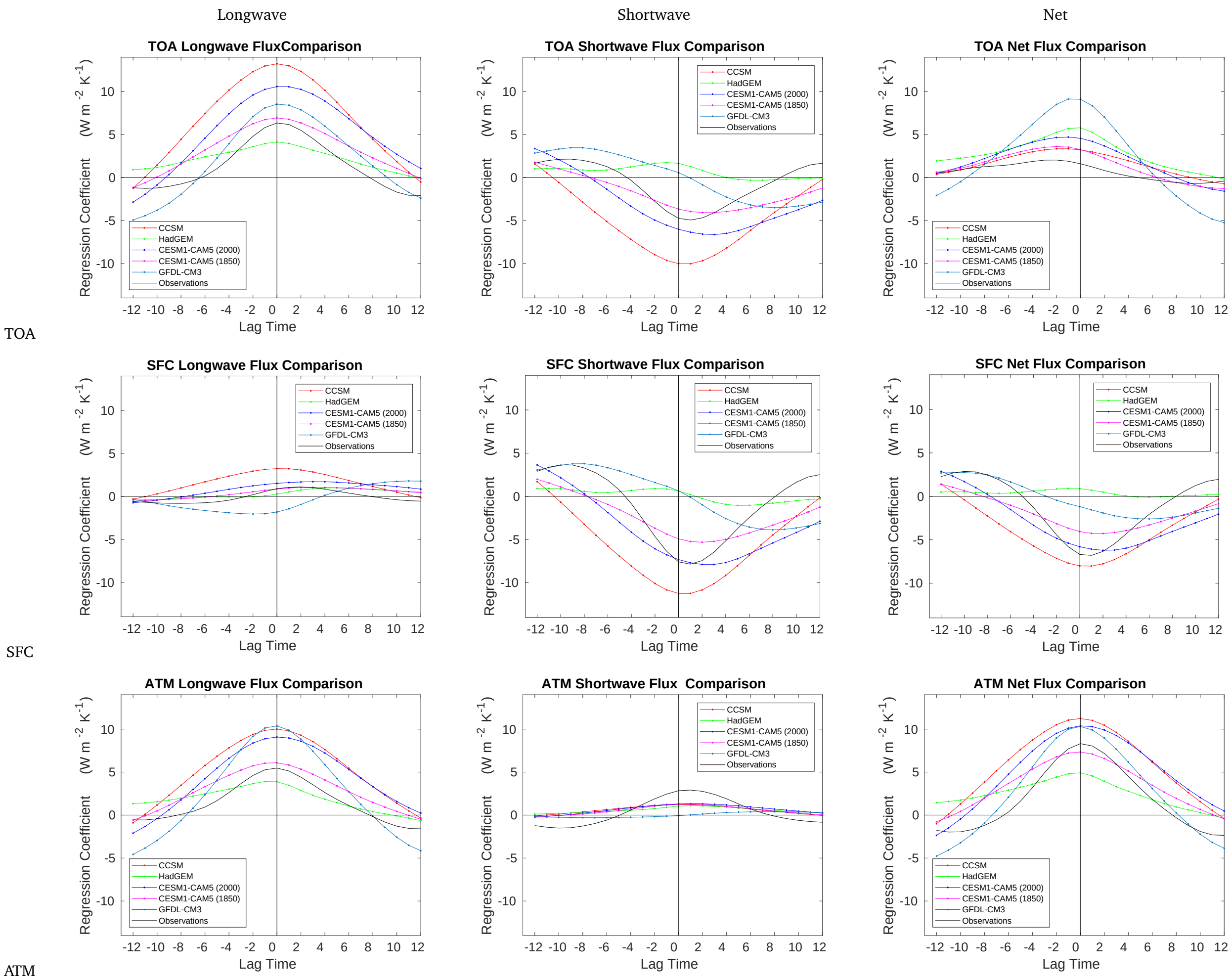

Figure 4.15: Like figure 4.14, but for the Ni no region mean [W m^{-2} K^{-1}].

that the positive bias is more due to the shortwave feedback being too “positive”.

In terms of overall pattern throughout the ENSO cycle, the largest discrepancy lies within the models’ estimates of the shortwave cloud radiative feedback. The CCSM simulation gives the best estimate of shape, while the shape of the GFDL simulation tends to follow a pattern opposite to what is seen in observations. The best visualisation of the shortwave discrepancy can be seen when we look at the atmospheric comparison between the observations and the models.

Figures 4.14 through 4.17 present new insights into the differences between the models, themselves, and observations. We see that the model fluxes to a good job of representing the overall pattern in both the tropical and Niño region means. Meanwhile, we

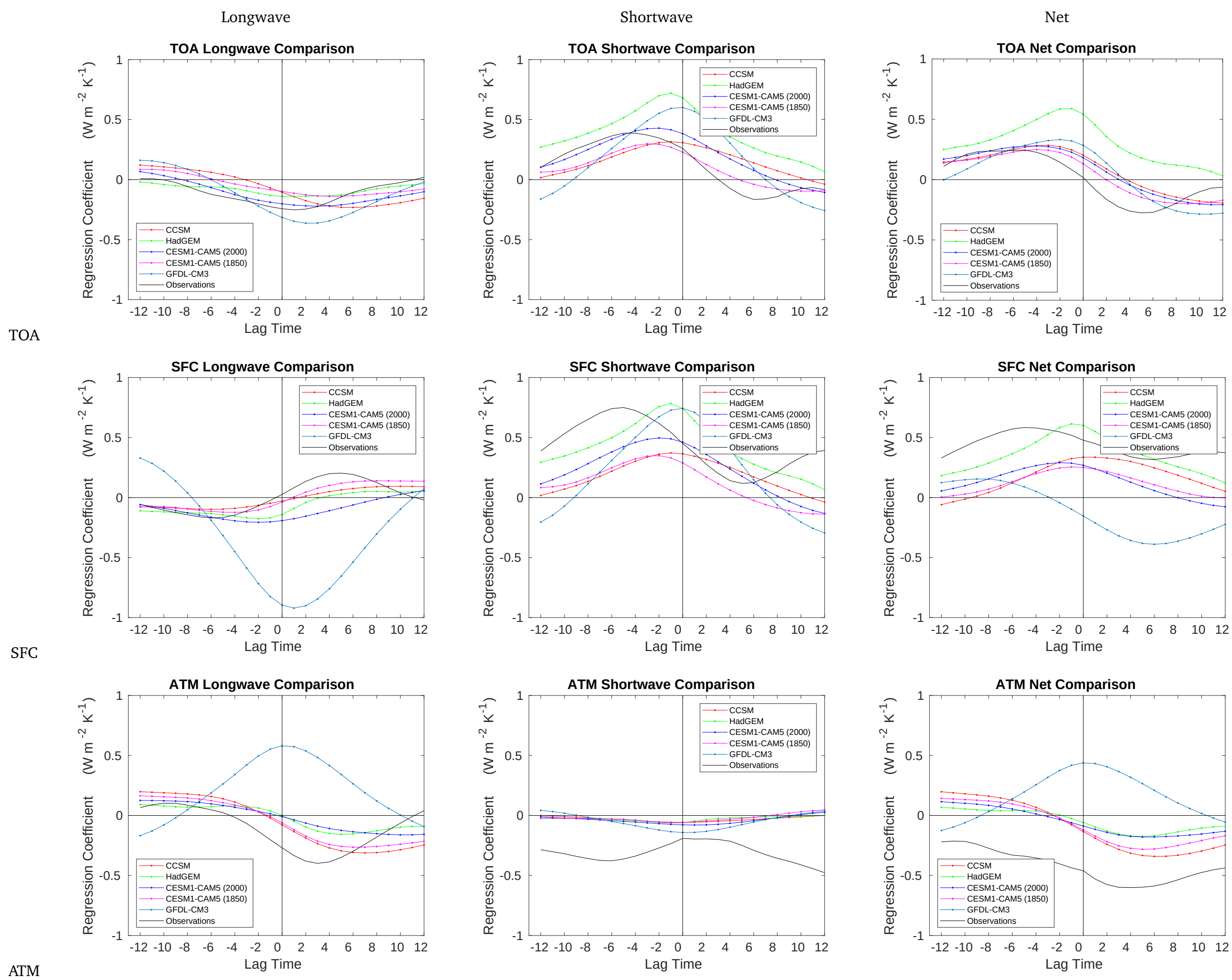

Figure 4.16: Like figure 4.14, but for the tropical mean cloud radiative feedback [W m^{-2} K^{-1}].

see that the cloud radiative feedback in the models does not accurately represent regional feedbacks. This result is consistent with the findings of [42] where they see that models consistently have larger regional anomalies when compared to observations.

4.5 Additional Discussion

One part of the model-observation discrepancy can come from the use of coupled GCMs, since the simulation of ENSO is dependent on both atmospheric and oceanic processes. As an alternative solution, we also considered the atmospheric (AMIP) model response to a

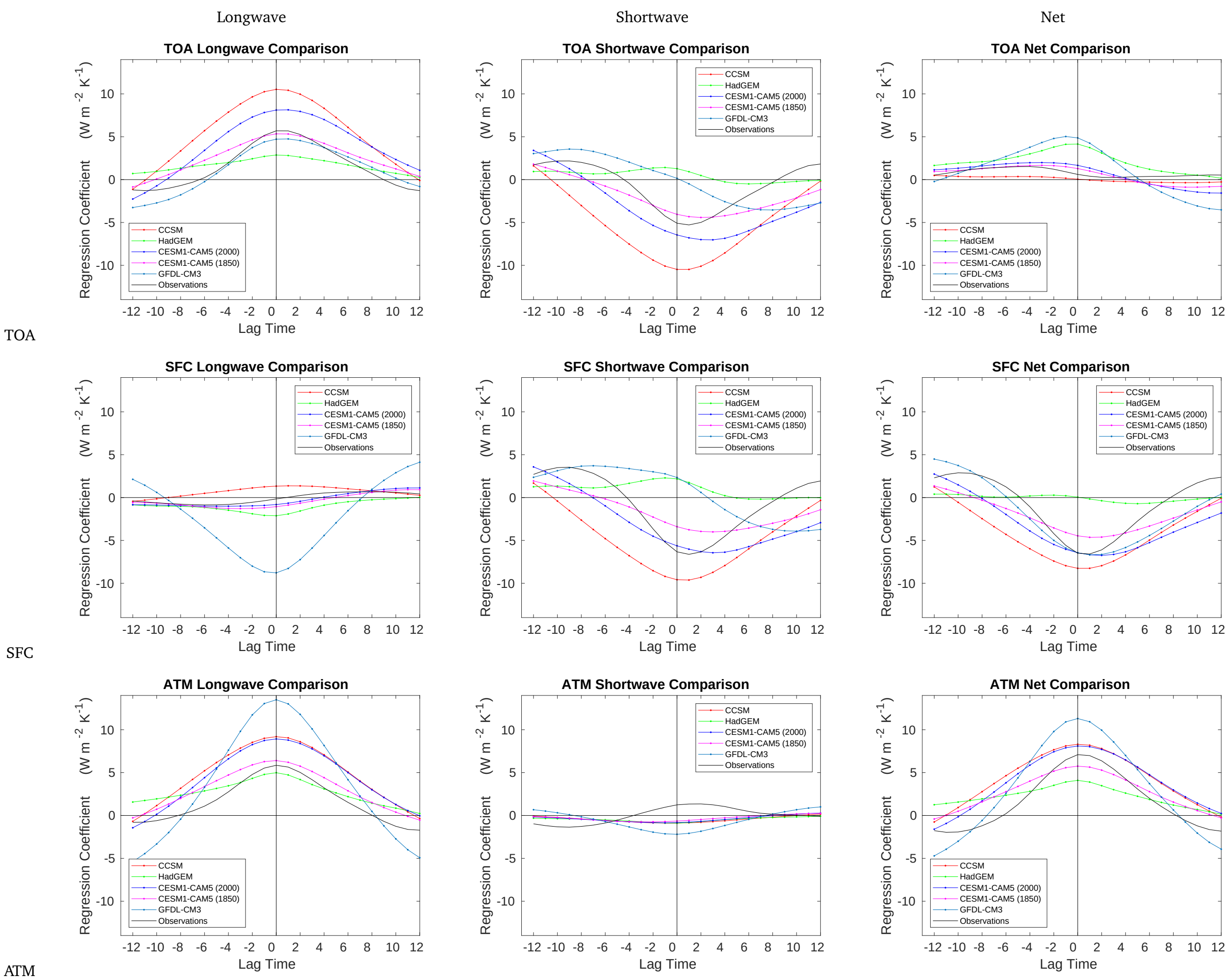

Figure 4.17: Like figure 4.14, but for the Niño mean cloud radiative feedback [W m^{-2} K^{-1}].

prescribed SST experiment. For this we use the Whole Atmosphere Community Climate Model (WACCM) with prescribed, observed SST from 1950-2008. Despite having a prescribed monthly mean SST, matching that of observations, figure 4.18 shows that a positive bias still exists in the eastern Pacific when we look at the net cloud feedback at TOA. At the surface, we also see a positive signal over the central Pacific in the longwave component which differs from both figures 4.2 and 4.13. Finally, the shortwave component in the atmosphere displays a positive bias which is more similar to that seen in figure 4.2. Overall, based on the results of this experiment, we can conclude that the use of a prescribed SST does not result in radiative feedbacks resembling those seen in observations and the positive bias seen in the coupled models at TOA is still present in atmospheric models.

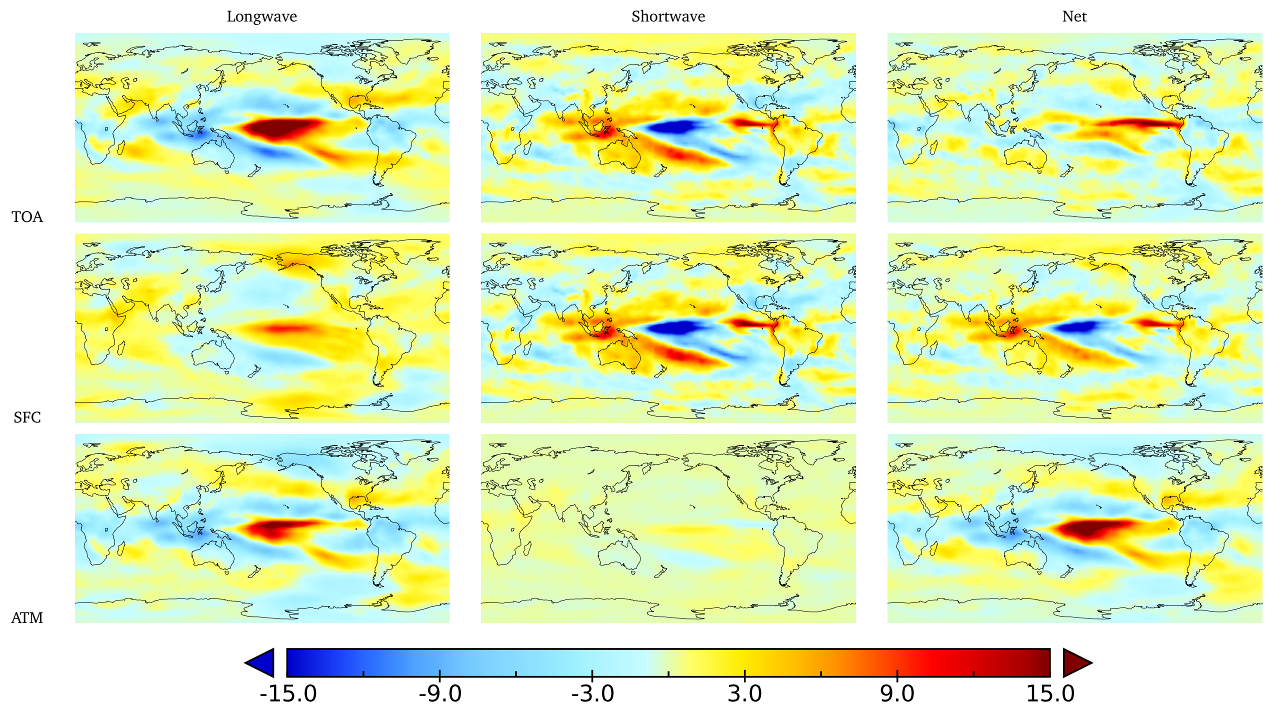

Figure 4.18: Cloud radiative effect of an AMIP prescribed SST experiment regressed to the Niño 3.4 region mean[W m^{-2} K^{-1}]

In section 3.2 we had mentioned the lengths of the various GCM time series's which are all much longer than the time series of the observations. Due to this fact, it is possible that the difference in timeseries length is a contributing factor in the model-observation discrepancy. Figures 4.19 and 4.20 plot the tropical and Niño region means, respectively, of cloud radiative feedback regressed to the Niño 3.4 index of the observations and models along with their corresponding 95% confidence intervals. When we look at the tropical mean curves and their standard deviations,figure 4.19, the observations agree with all of the models within one standard deviation. However, the Niño region mean is quite different. Figure 4.20 shows the Niño region mean and its standard deviation. Here, the observations do not agree with any of the models, within error. Thus, the length of the time series is not an important factor when considering the biases shown by the models over the entire tropical region, but when it is possible that the timeseries length plays a role in local discrepencies and biases.

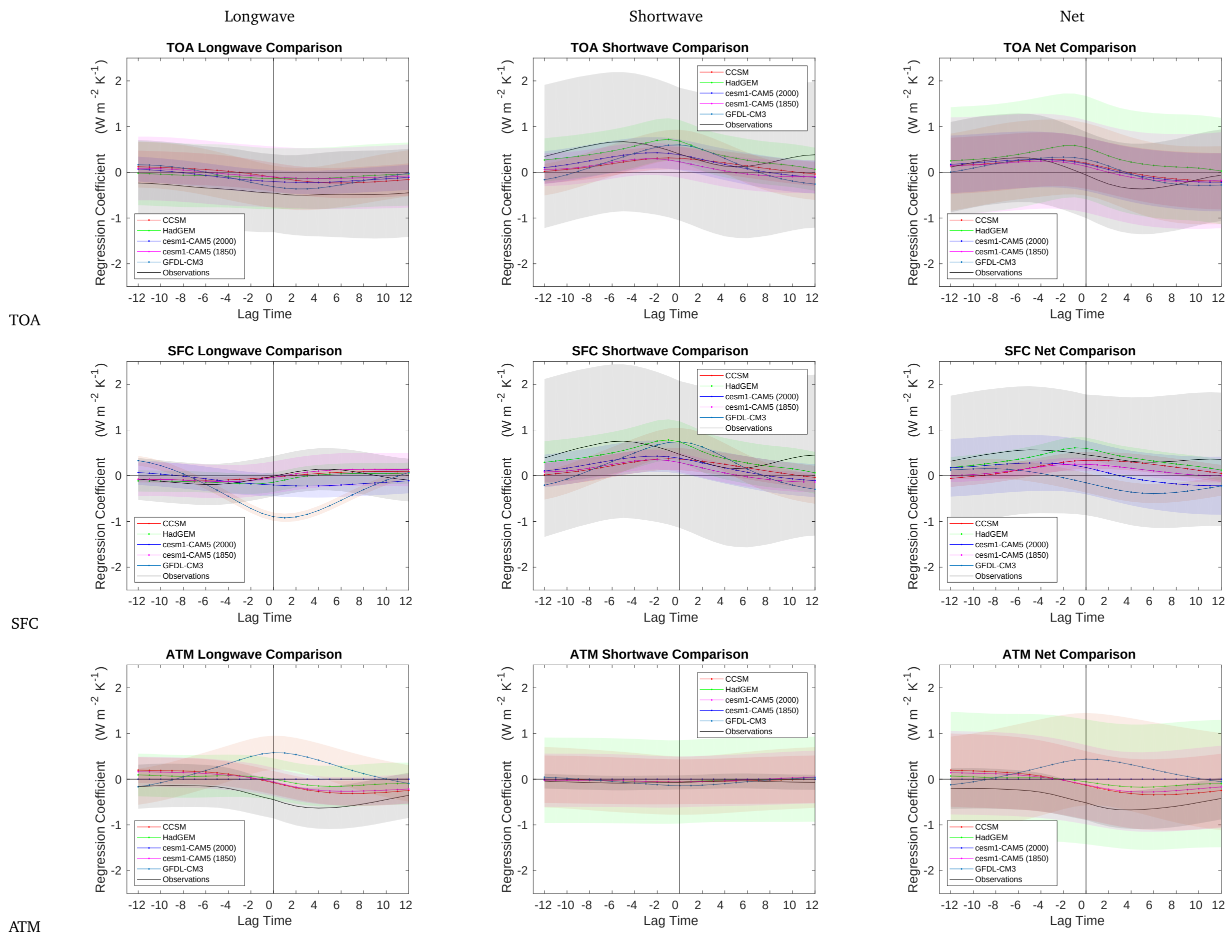

Figure 4.19: Lagged regression comparison between observations (black) and models ofthe tropical mean radiative feedback regressed to to the Niño 3.4 region mean SST with corresponding 95% confidence intervals [Wm^{-2} K^{-1}].

From the analysis presented above we learn a lot about feedback in the context of ENSO. From here, an interesting topic to discuss is the use of ENSO as an observable constraint on the climate sensitivity and its relevance to global warming. In order to discuss this, we can follow the same procedure outlined above while considering a 2xCO2 experiment, using CESM, and dividing by the global mean SST. We analyse the strength of the 2xCO2 cloud feedback and study its ENSO implications finding the cloud radiative anomaly and dividing by the global mean SST. Figure 4.21 shows that the global feedback pattern under a warming is significantly stronger. At TOA, the longwave feedback pattern

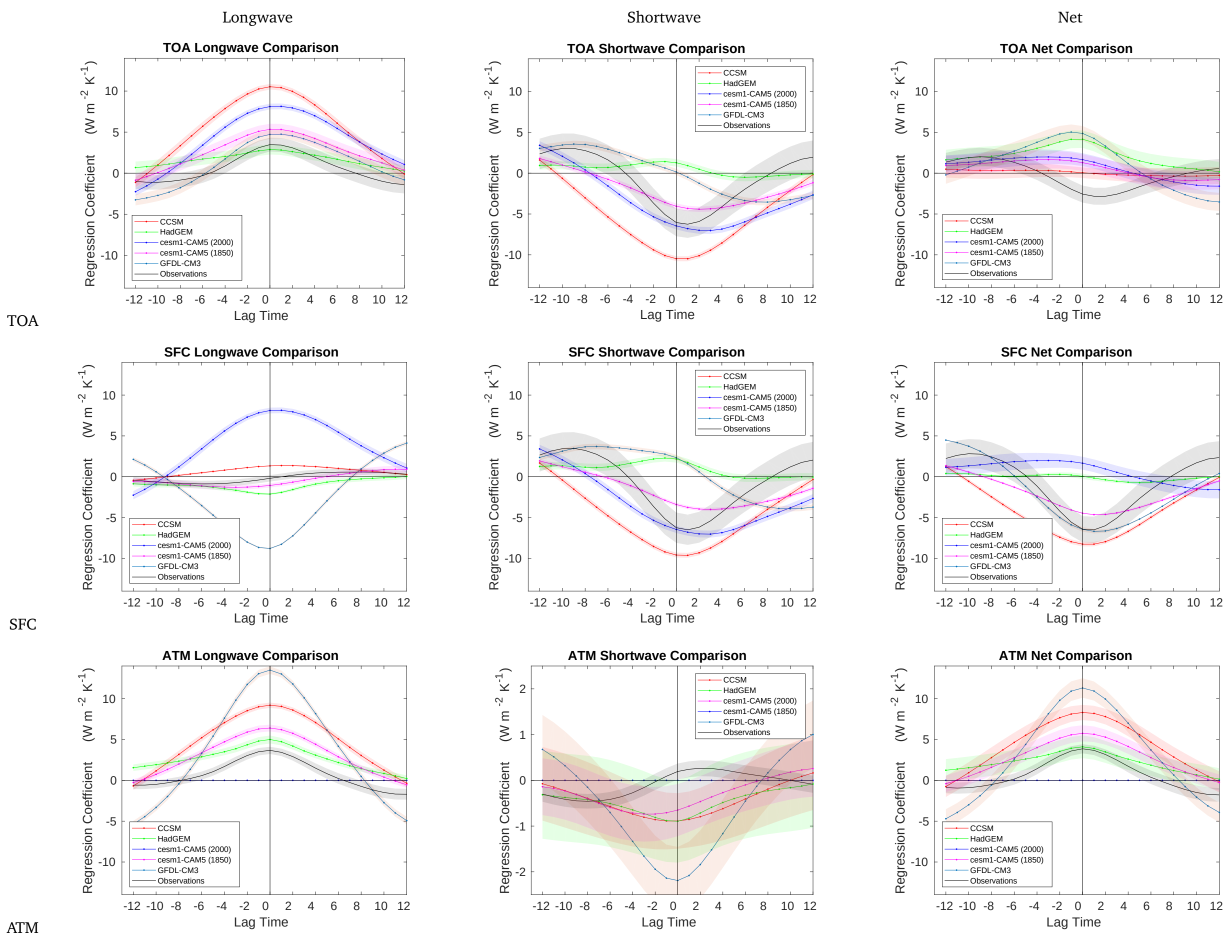

Figure 4.20: Like figure 4.19, but the Niño 3.4 mean regressed to the Niño 3.4 region mean[W m^{-2} K^{-1}]

still dominates the net feedback in the central Pacific, however this pattern is smoother and more neutral than the distinct bias seen in figure 4.8. This result is similar to what was seen in [3], where they saw that atmospheric model exhibited a smoother spatial distribution when compared to a coupled model.

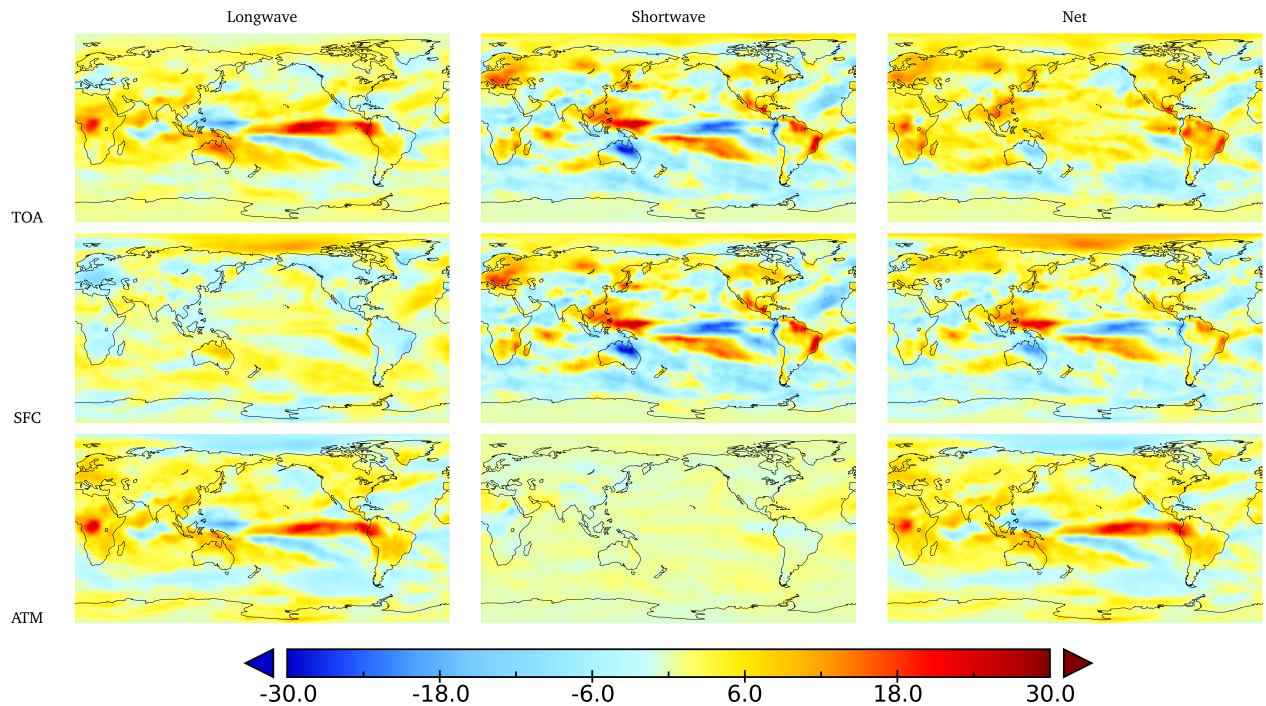

Figure 4.21: Annual mean 2xCO2 cloud radiative effect divided by the annual global mean SST [W m^{-2} K^{-1}]

Chapter 5

Conclusion

ENSO is a natural phenomenon that undergoes with a two to seven year cycle whose positive phase is called El Niño. Despite the constant changes, little is known about the role that radiation plays during ENSO. The purpose of this study was to use radiative kernels in order to gain an understanding of the role of radiation at TOA, the surface, and in the atmosphere. Furthermore, the study addressed and wished to better explain a known discrepancy between observations and models.

By using radiative kernels at TOA and at the surface, we were able to combine the two budgets to create an atmospheric budget. This is important since we have shown that a tropical mean radiation anomaly of 1 Wm^{-2} translates to a 3K temperature change for the whole atmospheric column. By performing a lagged regression, we can see the radiative, and cloud radiative feedbacks throughout different phases of ENSO. At TOA in the observations we observe that the tropical mean λ_{Net} transits from positive to negative at the peak of the El Niño event. This transition indicates that the cloud radiative feedback plays an important role in helping to build, and then maintain, a positive temperature anomaly.

The next part of this work looked at the CESM-CAM5 model in which all radiative gases were fixed at the year-2000 levels (CESM2000), and drew comparisons to the observed results. It was shown that this model does a good job at replicating the shape of the various feedbacks at TOA. However, difference exist between model and observation at the surface which have an effect on the atmospheric budget. We have shown that, throughout the ENSO cycle, the tropical mean cloud radiative feedback experiences only small perturbation - indicating that, in the model, the clouds play a minimal role during ENSO. However, in looking at global maps, a strong positive bias is visible at TOA and in the atmosphere.

To generalise the conclusions drawn by the CESM2000 experiment, the same analysis was performed on four other experiements and an inter-model mean and standard deviation were calculated for the tropical and Niño region means of both the flux and the cloud radiative feedback. In looking at the Niño region mean, the Net positive bias is apparent, but, contrary to previous ideas, we see that this bias is not only due to an overestimation of λ_{LW}, but also due to an underestimation of λ_{SW}.

Finally, as a compliment to the inter-model means and standard deviations shown, the lagged regression of the radiative and cloud radiative feedbacks are analysed to illustrate the inter-model differences and draw comparisons to observations. The most notable result is that the net positive bias exists across all models.

In conclusion, cloud radiative feedback plays an important role in different phases of ENSO. However, this role is minimal in the tropical mean of the models. In the Niño 3.4 region, the previously documented positive bias remains apparent in models representative of the CMIP5 model ensemble. We conclude that this bias is not only due to an overestimation of the longwave cloud feedback, but also due to an underestimation of the shortwave cloud feedback.

Bibliography

[1] Rebecca Lindsey. Global impacts of el niño and la niña. https://www.climate.gov/news-features/featured-images/global-impacts-el-ni%C3%B1o-and-la-ni%C3%B1a, 2016. Accessed:2017-07-10.

[2] Steve Graham. Clouds & radiation fact sheet : Feature articles. http://earthobservatory.nasa.gov/Features/Clouds/, March 2011. Accessed:2016-04-09.

[3] A. E. Dessler. Observations of Climate Feedebacks over 2000-10 and Comparisons to Climate Models. *Journal of Climate*, pages 333–342, 2013.

[4] Kevin E Trenberth. The definition of El Niño. *Bulletin of the American Meteorological Society*, 78(12):2771–2777, 1997.

[5] National Ocean Service. What are El Niño and La Niña. http://oceanservice.noaa.gov/facts/ninonina.html, March 2009. Accessed:2017-01-20.

[6] Tom Di Liberto. The Walker Circulation: ENSO's atmospheric buddy. https://www.climate.gov/news-features/blogs/enso/walker-circulation-ensos-atmospheric-buddy, August 2014. Accessed: 2017-01-20.

[7] NASA. What is El Niño anyway? http://spaceplace.nasa.gov/el-nino/en/, May 2014. Accessed:2017-01-20.

[8] D-Z Sun, T Zhang, C Covey, SA Klein, WD Collins, JJ Hack, JT Kiehl, GA Meehl, IM Held, and M Suarez. Radiative and dynamical feedbacks over the equatorial cold tongue: results from nine atmospheric gcms. *Journal of climate*, 19(16):4059–4074, 2006.

[9] De-Zheng Sun, Yongqiang Yu, and Tao Zhang. Tropical water vapor and cloud feedbacks in climate models: A further assessment using coupled simulations. *Journal of Climate*, 22(5):1287–1304, 2009.

[10] Gaby Rädel, Thorsten Mauritsen, Bjorn Stevens, Dietmar Dommenget, Daniela Matei, Katinka Bellomo, and Amy Clement. Amplification of el niño by cloud longwave coupling to atmospheric circulation. *Nature Geoscience*, 9(2):106–110, 2016.

[11] Graeme L. Stephens. Cloud feedbacks in the climate system: A critical review. *Journal of Climate*, 18:237–273, 2005.

[12] Roy W. Spencer and William D. Braswell. On the misdiagnosis of surface temperature feedbacks from variations in earth's radiant energy balance. *Remote Sensing*, 3(12):1603–1613, July 2011.

[13] RT Wetherald and S Manabe. Cloud feedback processes in a general circulation model. *Journal of the Atmospheric Sciences*, 45(8):1397–1416, 1988.

[14] Brian J Soden, Anthony J Broccoli, and Richard S Hemler. On the use of cloud forcing to estimate cloud feedback. *Journal of Climate*, 17(19):3661–3665, 2004.

[15] Robert D Cess, GL Potter, JP Blanchet, GJ Boer, AD Del Genio, M Deque, V Dymnikov, V Galin, WL Gates, SJ Ghan, et al. Intercomparison and interpretation of climate feedback processes in 19 atmospheric general circulation models. *Journal of Geophysical Research: Atmospheres*, 95(D10):16601–16615, 1990.

[16] RD Cess, MH Zhang, WJ Ingram, GL Potter, V Alekseev, HW Barker, E Cohen-Solal, RA Colman, DA Dazlich, AD Del Genio, et al. Cloud feedback in atmospheric general circulation models: An update. *Journal of Geophysical Research-Atmospheres*, 101:12791–12794, 1996.

[17] Brian J Soden, Isaac M Held, Robert Colman, Karen M Shell, Jeffrey T Kiehl, and Christine A Shields. Quantifying climate feedbacks using radiative kernels. *Journal of Climate*, 21(14):3504–3520, 2008.

[18] Karen M Shell, Jeffrey T Kiehl, and Christine A Shields. Using the radiative kernel technique to calculate climate feedbacks in ncar's community atmospheric model. *Journal of Climate*, 21(10):2269–2282, 2008.

[19] Jessica Vial, Jean-Louis Dufresne, and Sandrine Bony. On the interpretation of inter-model spread in CMIP5 climate sensitivity estimates. *Climate Dynamics*, 41(11-12):3339–3362, 2013.

[20] Eui-Seok Chung and Brian J Soden. An assessment of direct radiative forcing, radiative adjustments, and radiative feedbacks in coupled ocean–atmosphere models. *Journal of Climate*, 28(10):4152–4170, 2015.

[21] Yi Huang, Yan Xia, and Xiaoxiao Tan. Radiative feedbacks on global precipitation. *Journal of Geophysical Research - Atmosphere*, submitted.

[22] Langley ASDC User and Data Services Office. Earth radiation budget experiment (erbe) langley asdc project document. `https://eosweb.larc.nasa.gov/GUIDE/campaign_documents/erbe_project.html`, January 1996. Accessed:2017-07-12.

[23] Greg Kopp, George Lawrence, and Gary Rottman. The total irradiance monitor (TIM): science results. In *The Solar Radiation and Climate Experiment (SORCE)*, pages 129–139. Springer, 2005.

[24] Norman G Loeb, Bruce A Wielicki, David R Doelling, G Louis Smith, Dennis F Keyes, Seiji Kato, Natividad Manalo-Smith, and Takmeng Wong. Toward optimal closure of the earth's top-of-atmosphere radiation budget. *Journal of Climate*, 22(3):748–766, 2009.

[25] Shashi K Gupta, Nancy A Ritchey, Anne C Wilber, Charles H Whitlock, Gary G Gibson, and Paul W Stackhouse Jr. A climatology of surface radiation budget derived from satellite data. *Journal of Climate*, 12(8):2691–2710, 1999.

[26] V Ramanathan. Scientific use of surface radiation budget data for climate studies. *Surface Radiation Budget for Climate Application*, 1169:58–86, 1986.

[27] Kevin E Trenberth and Julie M Caron. Estimates of meridional atmosphere and ocean heat transports. *Journal of Climate*, 14(16):3433–3443, 2001.

[28] Yuanchong Zhang, William B Rossow, Andrew A Lacis, Valdar Oinas, and Michael I Mishchenko. Calculation of radiative fluxes from the surface to top of atmosphere based on ISCCP and other global data sets: Refinements of the radiative transfer model and the input data. *Journal of Geophysical Research: Atmospheres*, 109(D19), 2004.

[29] Robert D Cess, Ellsworth G Dutton, John J Deluisi, and Feng Jiang. Determining surface solar absorption from broadband satellite measurements for clear skies: Comparison with surface measurements. *Journal of Climate*, 4(2):236–247, 1991.

[30] Martin Wild, Doris Folini, Christoph Schär, Norman Loeb, Ellsworth G Dutton, and Gert König-Langlo. The global energy balance from a surface perspective. *Climate dynamics*, 40(11-12):3107–3134, 2013.

[31] Jean-Louis Dufresne and Sandrine Bony. An assessment of the primary sources of spread of global warming estimates from coupled atmosphere-ocean models. *Journal of Climate*, 21(19):5135–5144, 2008.

[32] Bruce A Wielicki, Bruce R Barkstrom, Edwin F Harrison, Robert B Lee III, G Louis Smith, and John E Cooper. Clouds and the earth's radiant energy system (CERES): An earth observing system experiment. *Bulletin of the American Meteorological Society*, 77(5):853–868, 1996.

[33] DP Dee, SM Uppala, AJ Simmons, Paul Berrisford, P Poli, S Kobayashi, U Andrae, MA Balmaseda, G Balsamo, P Bauer, et al. The ERA-Interim reanalysis: Configuration and performance of the data assimilation system. *Quarterly Journal of the royal meteorological society*, 137(656):553–597, 2011.

[34] Kevin E Trenberth, Yongxin Zhang, John T Fasullo, and Shoichi Taguchi. Climate variability and relationships between top-of-atmosphere radiation and temperatures on earth. *Journal of Geophysical Research: Atmospheres*, 120(9):3642–3659, 2015.

[35] James W Hurrell, Marika M Holland, Peter R Gent, Steven Ghan, Jennifer E Kay, Paul J Kushner, J-F Lamarque, William G Large, D Lawrence, Keith Lindsay, et al. The Community Earth System Model: a framework for collaborative research. *Bulletin of the American Meteorological Society*, 94(9):1339–1360, 2013.

[36] Stephen M Griffies, Michael Winton, Leo J Donner, Larry W Horowitz, Stephanie M Downes, Riccardo Farneti, Anand Gnanadesikan, William J Hurlin, Hyun-Chul Lee, Zhi Liang, et al. The GFDL CM3 coupled climate model: characteristics of the ocean and sea ice simulations. *Journal of Climate*, 24(13):3520–3544, 2011.

[37] Peter R Gent, Gokhan Danabasoglu, Leo J Donner, Marika M Holland, Elizabeth C Hunke, Steve R Jayne, David M Lawrence, Richard B Neale, Philip J Rasch, Mariana Vertenstein, et al. The community climate system model version 4. *Journal of Climate*, 24(19):4973–4991, 2011.

[38] C.D. Jones, J.K. Hughes, Nicolas Bellouin, S.C. Hardiman, G.S. Jones, Jeff Knight, Spencer Liddicoat, F.M. O'Connor, Robert Joseph Andres, Christopher Bell, et al.

The HadGEM2-ES implementation of CMIP5 centennial simulations. *Geoscientific Model Development*, 4(3):543, 2011.

[39] Ping Wang, Wouter H Knap, and Piet Stammes. Cloudy sky shortwave radiative closure for a Baseline Surface Radiation Network site. *Journal of Geophysical Research: Atmospheres*, 116(D8), 2011.

[40] Elena Yulaeva and John M Wallace. The signature of ENSO in global temperature and precipitation fields derived from the microwave sounding unit. *Journal of Climate*, 7(11):1719–1736, 1994.

[41] Climate Prediction Center Internet Team. Climate Prediction Center - Monitoring & Data: ENSO Impacts on the U.S. - Previous Events.

[42] Claire Radley, Stephan Fueglistaler, and Leo Donner. Cloud and radiative balance changes in response to ENSO in observations and models. *Journal of Climate*, 27(9):3100–3113, 2014.